Mechanism of the Reaction, $CH_4 + O(^1D_2) \rightarrow CH_3 + OH$, Studied by Ultrafast and State-Resolved Photolysis/Probe Spectroscopy of the $CH_4 \bullet O_3$ van der Waals Complex

C. Cameron Miller, Roger D. van Zee, & John C. Stephenson
National Institute of Standards and Technology,
100 Bureau Drive, Gaithersburg, Maryland 20899 USA

Abstract. The mechanism of the reaction $CH_4 + O(^1D_2) \rightarrow CH_3 + OH$ was investigated by ultrafast, time-resolved and state-resolved experiments. Short, ultraviolet pulses photolyzed ozone in the $CH_4 \bullet O_3$ van der Waals complex to produce $O(^1D_2)$. The ensuing reaction with CH_4 was monitored by measuring the appearance rate of OH(v=0,1; J, Ω, Λ) by laser-induced fluorescence, through the OH $A \leftarrow X$ transition, using short probe pulses. These spectrally broad pulses, centered between 307 nm – 316 nm, probe many different OH rovibrational states simultaneously. At each probe wavelength, both a fast and a slow rise time were evident in the fluorescence signal, and the ratio of the fast-to-slow signal varied with probe wavelength. The distribution of OH(v, J, Ω, Λ) states, $P_{obs}(v, J, \Omega, \Lambda)$, was determined by laser-induced fluorescence using a high-resolution, tunable dye laser. The $P_{obs}(v, J, \Omega, \Lambda)$ data and the time-resolved data were analyzed under the assumption that different formation times represent different reaction mechanisms and that each mechanism produces a characteristic rovibrational distribution. The state-resolved and the time-resolved data can be fit independently using a two-mechanism model: the sum of two Boltzmann distributions adequately represents $P_{obs}(v, J, \Omega, \Lambda)$, and the appearance of OH can be fit by two exponential rise times. However, these independent analyses are not mutually consistent. The time-resolved and state-resolved data can be consistently fit using a three-mechanism model. The OH appearance signals, at all probe wavelengths, were fit with times $\tau_{fast} \approx 0.2$ ps, $\tau_{inter} \approx 0.5$ ps and $\tau_{slow} \approx 5.4$ ps. The slowest of these three is the rate for dissociation of a vibrationally excited methanol intermediate (CH_3OH^*) predicted by statistical theory after complete intramolecular energy redistribution following insertion of $O(^1D_2)$ into CH_4. The $P_{obs}(v, J, \Omega, \Lambda)$ was decomposed into three components, each with a linear surprisal, under the assumption that the mechanism producing OH at a statistical rate would be characterized by a statistical prior. Dissociation of a CH_4O^* intermediate before complete energy randomization was identified as producing OH at the intermediate rate and was associated with a population distribution with more rovibrational energy than the slow mechanism. The third mechanism produces OH promptly with a cold rovibrational distribution, indicative of a collinear abstraction mechanism. After these identifications were made, it was possible to predict the fraction of signal associated with each mechanism at different probe wavelengths in the ultrafast experiment, and the predictions proved consistent with measured appearance signals. This model also reconciles data from a variety of previous experiments. To support the identification of the population distribution associated with the statistical OH channel, the distribution of energy in OH from the laser-induced, infrared-multiphoton dissociation of CH_3OH was analyzed.

PACS No: 82.20.Hf, 82.30.Eh, 82.40.Js, 82.50.Fv, 34.30+h

I. Introduction

The reaction between hydrocarbons and $O(^1D_2)$ is central to the chemistry of the atmosphere and combustion. As such, the mechanism and dynamics of the major reaction channel[1] of the simplest hydrocarbon, $CH_4(\tilde{X}\,^1A_1) + O(^1D_2) \rightarrow CH_3(\tilde{X}\,^2A_2'') + OH\ (X\,^2\Pi)$, have been extensively studied. The reaction is exothermic[2] ($\Delta H^\circ_{0\,K} = -182.$ kJ mol^{-1} = −15,240 cm^{-1}) with a rate constant close to a gas kinetic value and independent of temperature. Certain limiting, archetypical mechanisms can be envisioned for the reaction of O atoms with CH_4, including insertion/elimination, abstraction, and stripping. In the insertion/elimination archetype, the oxygen atom inserts into a C–H bond to form a vibrationally excited methanol intermediate (CH_3OH^*) that undergoes complete intramolecular vibrational energy redistribution (IVR) before dissociating. Both the distribution of energy in the fragments and the CH_3OH^* unimolecular dissociation rate would be expected to follow the predictions of statistical theory. For the abstraction mechanism, the oxygen atom would travel towards the methane molecule through a narrow tunnel along the carbon-hydrogen bond to extract a hydrogen atom and then recoil to form the hydroxyl radical. The reaction should be virtually instantaneous, and the distribution of rovibrational energy in the fragments would be colder than the statistical expectation. In the case of a stripping mechanism, the oxygen atom would fly by the methane molecule, snatching a hydrogen atom on the way. As with abstraction, a stripping reaction should be fast, but unlike an abstraction, should result in substantial rovibrational excitation in the hydroxyl product.

Nature is not confined to a single limiting case and early work supported parallel mechanisms. Initial evidence for a CH_3OH^* intermediate came from chemical quenching and matrix experiments[3,4,5] of the CH_4 and $O(^1D_2)$ reaction, which found that as the pressure in the reaction chamber increased, the quantum yield of CH_3OH increased. This observation was attributed to collisional stabilization of a CH_3OH^* intermediate. However, even in a liquid argon matrix some OH was formed, suggesting that at least a fraction of the product formed through an abstraction mechanism. Park and Wiesenfeld[6] studied the OH rovibrational product states from several hydrocarbons and concluded, that in the case of methane, most of the OH was characterized by a nonstatistical distribution. They postulated, however, that all the OH passed through a methanol intermediate, with most dissociation occurring prior to complete IVR. This conclusion was consistent with Luntz's earlier conjecture that most OH was formed by the latter mechanism, although OH in low rotational levels was formed by an abstraction mechanism. Sub-Doppler spectroscopy[7,8,9,10,11] has shown that OH(v=0) was scattered nearly isotropically in the center-of-mass frame, but with some backward asymmetry, again suggesting both a long-lived

intermediate and a reacting complex with a lifetime less than one rotational period. By comparison to OH, little is known about the CH_3 product. Absorption spectra[12] recorded with an infrared diode laser have been used to determine the nascent distribution of the out-of-plane bend (ν_2). It was found that v=0 was the most populated level of that mode, with monotonically decreasing population up to v=4. This measured distribution was significantly colder than an unconstrained, statistical prior distribution. Multiphoton ionization spectra[13,14] of the out-of-plane bend and symmetric stretch also suggested that there was comparatively little vibration excitation in the CH_3 fragment, though because the Franck-Condon factors and autodissociation rates of the excited state were unknown, no quantitative conclusions could be reached. An *ab initio* calculation[15] of the potential energy surface for the CH_4 + O reaction suggested that insertion-, abstraction-, and stripping-like mechanisms were possible. Although inconclusive, these investigations suggest complicated reaction dynamics.

Although OH and CH_3 are the major products (estimates vary from 69 % – 96 %), several minor products have also been identified for reactive collisions between CH_4 and $O(^1D_2)$. Figure 1 shows a correlation diagram indicating the energetics for various channels. Primary H atom production has been studied by laser-induced fluorescence experiments.[16,17,18] Whether the co-fragment was CH_3O or CH_2OH was controversial until recent crossed molecular beam experiments[19,20] found CH_2OH + H to be the second most probable channel. Most of the H atom product is isotropically scattered, though about a tenth is back scattered. This finding supports parallel mechanisms for this channel. The beam experiments also found that H_2CO + H_2 are primary products. All the H_2 was found to be isotropically distributed, and this channel was concluded to evolve through a CH_3OH^* intermediate after complete IVR. The methoxy radical has also been reported to be a direct product of this reaction, although whether methoxy is a direct product is unresolved. Because the O–H bond is not the weakest bond in the molecule, this would imply dissociation of an intermediate in which energy has not fully randomized. In addition, the reaction to form CH_2 (ã) + H_2O as minor primary products has been reported.[20,21,22] The observations about these minor products imply that dissociation of a methanol intermediate after energy randomization is the most important mechanism leading to their formation.

We previously reported preliminary findings from experiments aimed at further elucidating the mechanism of the primary reaction channel. An ultrafast laser system was used to measure the OH production as a function of time following ultrafast photolysis at 267 nm of the CH_4•O_3 van der Waals complex.[23] Prompt dissociation of ozone produces $O(^1D_2)$, which then reacts with the neighboring CH_4 to form OH. This reaction was monitored by measuring OH laser-induced fluorescence, through the OH

$A(^2\Sigma) \leftarrow X(^2\Pi)$ transition, as a function of photolysis/probe delay. Initiating the reaction in a cluster provides a clear time-zero against which to measure the appearance of the reaction products.[24,25,26] A single exponential rise with a time constant of several picoseconds adequately fit the OH(v=0,J) states probed in those experiments. This appearance rate was consistent with the rate of dissociation of CH_3OH^* predicted by statistical rate theory. Given the time resolution and signal-to-noise of that experiment, we concluded that any prompt OH channel produced less than 20 % of that probed. We also determined the rotational state distributions in the cluster reaction and found them quite similar to those of the free, bimolecular reaction, an observation which Wada and Obi[27] subsequently confirmed and which suggests that the cluster environment replicates the dynamics of the free bimolecular reaction.

The present article expands on our preliminary study and reports important, new findings. Improved time resolution, increased signal-to-noise, and the ability to probe more OH(v=0) rotational states and OH(v=1) made these new time-resolved results possible. The appearance of OH was measured at six probe wavelengths spanning the OH(v=0, 1) manifolds. The new data clearly show, in addition to the previously reported statistical channel, OH formed by much faster mechanisms. We have also measured the OH(v=0, 1) rotational state distribution again.

In this paper, the time- and state-resolved data are analyzed with the idea that different formation times represent different formation mechanisms and that each mechanism produces a unique and characteristic distribution of rovibrational energy in the products. Because of the complexity of the OH spectrum and the spectral breadth of the short pulses, the probe laser pulse interacts with many different rovibrational levels of OH, which complicates the analysis. A two-mechanism model fits either rovibrational distribution data or rise time data well, but fails to provide a coherent, internally consistent picture of the reaction. The data are more consistently fit by a model with three mechanisms. One is the previously reported slow, statistical dissociation of CH_3OH^* ($\tau_{slow} \approx 5.4$ ps) characterized by a statistical population distribution. A second channel creates OH much more quickly ($\tau_{inter} \approx 0.5$ ps) and with more rovibrational excitation. We ascribe this to the decay of a CH_4O^* before complete IVR. The third channel is extremely fast ($\tau_{fast} \approx 0.2$ ps) with a cold population distribution, characteristic of an abstraction reaction. This third channel could involve $O(^1D_2)$ or $O(^3P_j)$ atoms formed either directly in the O_3 photolysis or as the result of a curve crossing in the reaction entrance channel. The product state distribution is decomposed into three components using a surprisal analysis and subject to the assumption that the slowest channel produced product with a statistical distribution of energy in the

products. In Appendix A this three-channel model is compared to previous studies and found to reconcile seemingly different observations. Appendix B presents and analyzes data on the carbon dioxide laser-induced, infrared-multiphoton dissociation (IRMPD) of methanol. These data show that vibrationally excited methanol in which energy is randomized before dissociation does produce OH with a statistical energy distribution. This observation bolsters the assumption that the mechanism with the slowest rate would also produce OH with a statistical energy distribution.

II. Experimental Apparatus & Procedures

The light source for the ultrafast photolysis/probe experiment consisted of a passively mode-locked, titanium doped sapphire ($Ti:Al_2O_3$) laser oscillator that produced transform limited, 70 fs pulses centered at 800 nm. The pulses were stretched to >200 ps, amplified to 2 mJ at a repetition rate of 20 Hz in a $Ti:Al_2O_3$ regenerative amplifier, further amplified to 20 mJ in a second $Ti:Al_2O_3$ rod using a three pass configuration, and then compressed to 100 fs. The amplifier rods were pumped by 10 ns, 532 nm pulses from a Nd^{3+}:YAG laser. The 267 nm photolysis light was generated by first doubling this compressed 800 nm light and then summing the resulting 400 nm light with residual 800 nm light. The probe was generated by focusing part of the 800 nm light into a cell containing deuterated water to create a white light continuum, which was passed through an interference filter to select light near 500 nm. This seed pulse was amplified in three, 1 cm dye cuvettes, which were pumped by 355 nm pulses from a second Nd^{3+}:YAG laser. This light was then summed with 800 nm light in a 0.5 mm KH_2PO_4 (KDP) crystal to give wavelengths between 307 nm – 316 nm ($\Delta\lambda_{FWHM} \approx 1.6$ nm). The interference filter was tilted to tune the center frequency of the transmitted light. Typically, 20 μJ per pulse of photolysis light and 15 μJ per pulse of probe light were used. The orthogonally polarized pump and probe beams were combined on a dichroic mirror and propagated collinearly through the beam chamber. At fluences for which data was obtained, the laser induced fluorescence (LIF) signal was linear in photolysis and probe pulse energy, and no multiphoton effects were observed.

The supersonic expansion in which the van der Waals complexes were formed, and the LIF detection apparatus were the same as in previous experiments.[23,28] The clusters formed in a supersonic expansion from reactants diluted in a 9:1 mixture of Ne:He. A 6% mix of O_3 in Ne:He flowed through one calibrated flow controller, pure CH_4 through another, and additional Ne:He through a third. The gases mixed just upstream of the pulsed valve, yielding a typical mix of 81 % Ne, 9 % He, 8 % CH_4, and 2 % O_3. Prior to use, gaseous O_3 was purified by distillation from liquid O_3. The total stagnation pressure was ≈310 kPa, and the chamber pressure was ≈1 mPa when the nozzle was pulsing. Under

these mixture conditions, the OH signal was linear in the methane and ozone mole fraction. Additional evidence that the OH is formed in $CH_4 \bullet O_3$ clusters rather than larger clusters has been presented previously. At typical laser fluences, no signal was observed when either the methane or the ozone was removed from the expansion. The lasers, focused to a ≈1.5 mm spot, intersected the molecular beam 8 mm downstream from the throat of the expansion.

Proper analysis of the rise curves demands an accurate measurement of the time of photoinitiation of the reaction. This time was determined by measuring the photolysis/probe cross-correlation by difference frequency mixing in a 0.1 mm KDP crystal, generating ≈1.9 μm light. To make this measurement, the Fresnel reflections from the front surface of the lithium fluoride, chamber entrance-window passed through a second, lithium fluoride window identical to the chamber window. The difference frequency light was then generated in the KDP crystal, which was located at a point conjugate to the probe region in the chamber. The Gaussian full-width at half-maximum of the cross correlation was routinely ≈200 fs. Accounting for the dispersion of air (1.0 fs cm^{-1}) and the dispersion of the KDP crystal (8 fs), time-zero could be determined to within 5 fs. To test this clocking apparatus, two additional experiments were carried out. First, a second 0.1 mm KDP crystal was placed in the vented chamber at the region of interaction, and the two cross-correlations were compared. The cross-correlations were aligned in time to ≈5 fs. Second, the LIF of OH formed by 267 nm photodissociation of hydrogen peroxide was measured. The reaction $H_2O_2 \rightarrow 2OH$ is known to be prompt.[29,30,31,32] To make these measurements, vapor from a mixture of 70 % H_2O_2 in water flowed through the chamber at a pressure of ≈13 Pa. The rise curve of OH(v=0) LIF from this reaction was indistinguishable from the integral of the laser cross-correlation, except shifted in time by a delay due to the separation time of the OH fragments. The observed shift in time for the data set with probe laser centered at 308.9 nm is 25 fs ± 15 fs. Using a standard approach,[33] we calculated a shift to be 30 fs. Therefore, the time-zero from the H_2O_2 experiments was consistent with the value measured using the crystal. The rise time of OH from the prompt dissociation of H_2O_2 is compared to the fastest observed formation time of OH from the $CH_4 \bullet O_3$ cluster experiment in Fig. 2. This figure illustrates that the time resolution was sufficient to determine even the fastest OH formation rates from the cluster. To the best of our knowledge, this represents the fastest temporal resolution with which the dissociation of H_2O_2 has been measured.[29]

The detection system was a photomultiplier tube perpendicular to the laser beams with two condensing doublet lenses to collect and image the fluorescence. Colored glass filters blocked stray

photolysis light and wavelengths longer than 400 nm. On every laser pulse, gated boxcar integrators collect four channels of data: LIF from OH, the energy of the photolysis and probe beams, and signal from the photolysis/probe cross-correlation.

For the state-resolved photolysis/probe experiments, the fourth harmonic (266 nm, ≈1 mJ cm^{-2}, 7 ns) of a Nd^{3+}:YAG was used to photolyze the ozone. The second harmonic of another Nd^{3+}:YAG laser pumped a dye laser. The dye laser's second harmonic was the source (≈10 μJ cm^{-2}, $\Delta\nu_{FWHM}$ ≈ 0.3 cm^{-1}) to probe the OH fragments through the (0,0) and (1,1) bands of the $A(^2\Sigma) \leftarrow X(^2\Pi)$ system.[34] The supersonic expansion and LIF detection apparatus were those used in the ultrafast measurements. In the state-resolved experiments, it was possible to vary the photolysis/probe delay time in 10 ns steps. The signal rose sharply during the initial 20 ns after photolysis, following the integral of the temporal cross-correlation between the photolysis and probe lasers. The signal remained constant for the next 50 ns – 80 ns and then rose slowly or declined slowly, depending on the rovibrational state measured, as a result of collisional relaxation of OH. The data reported here were measured with a 30 ns delay.

The observed spectra were normalized to variations in the photolysis and probe laser fluences and to the intensity of the $P_1(15)$ line which was remeasured after scanning 2 nm. The normalized spectra were simulated by Lorentzian line shapes to determine the line intensities of overlapping lines. For hydroxyl in the $A(^2\Sigma)$ state, significant autodissociation occurs for rotational states, $N \geq 25$ in the v=0 level and $N \geq 15$ in the v=1. All rotational states autodissociate for $v \geq 2$. Because the diagonal bands were probed, only OH(v=0,1) could be detected. In determining populations from LIF line intensities, we corrected for the fluorescence quantum yield of the specific quantum levels,[35] but do not report populations if the correction was ≥50 %. Division by the Einstein B coefficients[36] converts intensities to relative populations. Results from independent measurements were then averaged.

III. Results and Discussion

Product-State Distributions. In order to understand the OH appearance measurements, one must understand the form of the product-state distribution and the extent to which the probe laser power spectrum encompasses the absorption spectrum of the product. Figure 3 shows a portion of an OH spectrum following 267 nm photolysis of the $CH_4 \bullet O_3$ cluster. Superimposed on the state-resolved spectra is a representation of the power spectrum of the probe laser at 312 nm. This figure illustrates how the probe pulses overlap many different rovibrational transitions. The population distribution, $P_{obs}(v, J, \Omega, \Lambda)$, the probability of OH being formed in a particular quantum state, was derived from the LIF spectra, such as that shown in Fig. 3. Hydroxyl has two spin-orbit states labeled by the quantum

number Ω = 1/2, 3/2.[37,38] The lower f_1 ($^2\Pi_{3/2}$) and the upper f_2 ($^2\Pi_{1/2}$) state are separated by 126 cm^{-1} for the lowest rotational level. The splitting decreases with increasing rotational excitation. Each spin-orbit state, in turn, is split into Λ-doublet components, labeled A′ and A″, which vary by ~0.2 % of the rotational energy for all rotational states probed in this experiment. As N increases, the orbital of the unpaired electron in the A′ state becomes localized in the plane of the molecular rotation, while for the A″ the electron orbital becomes localized perpendicular to the plane.[37] Because these four unique fine-structure states are not equally populated and the distributions may be related to the reaction mechanism, the population distribution for each state in both v=0 and v=1 is displayed in Fig. 4.

The populations presented in Fig. 4 agree well with those that we reported earlier.[28] A striking feature of these data is that the f_1 and f_2 levels of the lowest rotational levels are unequally populated, with more population in the f_1 state. An obvious explanation is that after the reaction the OH has undergone collisions in the beam, with rotational relaxation causing excess population in the states of lowest energy. However, a study of the LIF from these levels as a function of photolysis/probe delay time is consistent with the distributions being unaffected by collisions. Additional tests were performed by moving the laser crossing region from 8 mm to 20 mm downstream of the expansion nozzle, thereby, reducing the number density and the collision rate by a decade. The populations determined at 20 mm showed no difference from the populations determined at 8 mm. These observations suggest that post-dissociation collisions do not affect the $P_{obs}(v, J, \Omega, \Lambda)$ reported here.

Time-Resolved Data. The time evolution of the OH concentration following femtosecond 267 nm photolysis of the CH_4•O_3 van der Waals complex is shown in Figs. 4 and 5. The signal is plotted as a function of photolysis/probe delay time, t_d, at six different probe wavelengths. Figure 6 shows the early time data on a higher resolution scale. The traces are the averages of eight to ten scans, each of which was acquired during about half an hour. Consecutive scans were acquired from long to short delay time, then from short to long delay time. The data was collected from 1 ps before reaction initiation to 80 ps after reaction initiation. The most striking feature of the data is that both fast (<1 ps) and slow (≈5 ps) formation times are obvious in the rise curves. The fraction of OH formed with the fast or slow rate depends on probe wavelength. Because different wavelengths probe different groups of OH(v, J, Ω, Λ) states, this shows that different OH(v, J, Ω, Λ) levels have different formation rates. The fit of the time- and state-resolved data to particular models is discussed below.

One possibility for different rise times is that the signal arises from more than one reaction. A number of tests were undertaken to discount this possibility. First, the lifetime of the fluorescence signal

was observed to decay by one neper in ≈0.8 μs, which is the lifetime of the OH $A(^2\Sigma)$ state. Furthermore, no signal was detected when the ultrafast probe laser was detuned from the OH $A(^2\Sigma) \leftarrow X(^2\Pi)$ resonance. These observations support attribution of the observed signal to fluorescence from the OH $X \leftarrow A$ transition. Second, the fluorescence signal disappeared if either CH_4 or O_3 was withheld from the plenum. The CH_4 reagent had a stated purity of 99.999 %, so an impurity in that gas seems an improbable source of the observed OH. These observations suggest that the observed OH signal arises from a reaction between CH_4 and O. Third, the mole fractions of CH_4 and O_3 were independently varied over an order of magnitude while maintaining a constant backing pressure. While the overall LIF intensity did change linearly with mole fraction, the ratio of fast to slow components and the reaction rate varied by <5 %, the precision with which the fast-to-slow ratio can be determined from these data. In another test, the mole fraction of CH_4 and O_3 were fixed as the backing pressure was varied from 275 kPa to 345 kPa. Again, the ratio of fast-to-slow components and the reaction rate for each varied by less than five percent. Both of these observations support the idea that the reaction involves the $CH_4 \bullet O_3$ complex, because the density of larger clusters, $(CH_4)_m(O_3)_n$, would be expected to increase rapidly with increasing reagent concentration or plenum pressure. Finally, almost all of the OH probed on a picosecond-time scale comes from cluster reactions and not subsequent reactive collisions. An upper limit on the OH formation rate, *k*, from bimolecular collisions can be estimated using the formula,

$$k = \rho \sigma_r v \tag{1}$$

where ρ, the number density of CH_4 in the molecular expansion is $\approx 1.4 \times 10^{16}$ molecules cm^{-3}, the reactive cross section, σ_r, is ≈0.20 nm^2, and the relative velocity, *v*, is $\approx 6 \times 10^4$ cm s^{-1}. These numbers predict a reaction time of ≈0.5 μs, about $10^5 - 10^6$ times slower than the rise times reported here. Together, this evidence suggests that the time-resolved data represent the formation rates of OH from the $CH_4 \bullet O_3$ complex.

Comparison of the magnitude of the fluorescence from the cluster photolysis to that from a known pressure of flowing H_2O_2 provides an estimate of the quantum yield of formation of OH from $CH_4 \bullet O_3$. For both experiments,

$$LIF = \Phi^{OH} \rho \sigma(\lambda) P_{detect} \tag{2}$$

where Φ^{OH} is the quantum yield for OH formation, ρ is the density of the reactants, $\sigma(\lambda)$ is the wavelength dependant absorption cross section of the species initiating the reaction and P_{detect} is the

probability of detecting the OH formed. The value of these quantities for the hydrogen peroxide reaction are $\Phi^{OH} = 1.6$,[39] $\rho = 10^{15}$ molecules cm^{-3}, and $\sigma(267\ nm) = 9 \times 10^{-20}$ cm^{-2}.[40] From the known rovibrational distributions of OH, the relative probability of detecting the OH from the two experiments is estimated. For H_2O_2 photolysis, all OH is formed in the v=0, with little rotational excitation (≈1050 cm^{-1}).[41,42,43,44,45,46] In contrast, for the $CH_4 + O(^1D_2)$ reaction only about a quarter of the OH is formed in the v=0 level,[6] and it is formed with about three times more rotational energy than that from H_2O_2. Because of this difference in the rovibrational distributions, when the ultrafast laser is tuned to 310 nm, a wavelength that probes only OH in v=0 with moderate-J, it is ten times more likely to detect OH from H_2O_2 than OH from CH_4•O_3. For the CH_4•O_3 reaction, the OH quantum yield is the quantity to be estimated. The absorption cross section for free O_3 [$\sigma(267\ nm) = 9 \times 10^{-18}$ cm^{-2}][47] should be an adequate estimate of the absorption cross section in the cluster. The density of clusters in the beam was assumed to be ≈10 % of the O_3 pressure ($\rho \approx 4 \times 10^{14}$ clusters cm^{-3}). This estimate is based on previous studies of the NO dimer in this laboratory[48] showing that a dimer concentration greater than 10 % of the monomer produced higher order clusters, causing the signal to become nonlinear. The O_3 pressure in our expansion was just below that for which the signal became nonlinear, which we assume indicates a CH_4•O_3 cluster concentration of 10%. Clearly, this estimate could be in error. The measured signals for both H_2O_2 and CH_4•O_3 photolysis were comparable and from the quantities indicated one estimates the quantum yield for OH production from the cluster to be ≈0.4 following 267 nm photolysis. This calculation suggests that the cluster geometry does not impose severe dynamical constraints on the reaction.

Data Analysis. Above, we saw that the rise time data clearly contained fast and slow components the ratio of which depended upon the probe wavelength. The time- and state-resolved data are analyzed in this paper with the idea that more than one reactive mechanism produces OH, and that each mechanism has a characteristic formation rate and population distribution. The objective of our analysis is to decompose the observed population distribution into a set of distributions, each representing a different reactive mechanism with a unique formation time. This decomposition must be able to predict the fraction of population from each mechanism probed at each wavelength in the ultrafast experiments.

The first attempt at analysis assumes that only two channels contribute. The time-resolved data is taken as the sum of two exponentials, so that at each probe wavelength, the LIF time dependence is fit to the following functional

$$LIF(t_d) = X_i(t_d) \otimes \left[C_i^f \times OH_f(t_d) + \left(1 - C_i^f\right) \times OH_S(t_d) \right] \quad (3)$$

where $X_i(t_d)$ is the measured cross-correlation at photolysis-probe delay time t_d, $\otimes$ denotes convolution, C_i^f is the fraction of fast OH_f probed at wavelength and (1-C_i^f) is the fraction of slow OH_s The index *i* designates the six different probe wavelengths. The time evolution of the signal also is proportional to the OH number density at time t_d:

$$OH_f(t_d) = 1 - Exp(-t_d/\tau_f), \text{ and} \quad (4a)$$

$$OH_S(t_d) = 1 - Exp(-t_d/\tau_s) \quad (4b)$$

where τ_f and τ_s are the fast and slow formation time constants, respectively, and $OH_{f/s}(t_d) = 0$ for $t_d < 0$. That is, we assume every OH(v, J, Ω, Λ) has both a fast and slow formation time and these are the same for all quantum states, although the ratio of population formed by each mechanism may be different for every state.

The energy of the OH(v, J, Ω, Λ) states being probed is not related to the probe laser wavelength in any simple manner. The shortest wavelengths probe only OH(v=0). At 307.3 nm, the laser probes many rotational levels, primarily R branch bandheads, of the f_1 and f_2 states. The strong, low-J, Q and P branch lines of f_1 and some higher-J's of the R branch are probed at 308.8 nm. When the probe laser is tuned to 310.7 nm, the P and Q branch lines of intermediate-J are probed for f_1 and f_2. The other wavelengths probe a mixture of v=0 and v=1 levels. The fraction of OH(v = 1) states being probed increases with wavelength, and for probe wavelengths between 308.8 nm and 316.5 nm, the average energy of the OH being probed increases uniformly. All six data sets were fit to Eq. (3) simultaneously by varying the six C_i^f coefficients, τ_f and τ_s. The resulting C_i^f coefficients are shown in Fig. 7 (circle symbols). The fit to the time-resolved data and the residuals are displayed in Fig. 6. The fraction of fast OH lies between 0.23 – 0.69, depending on the probe wavelength and thereby the set of rovibrational states being probed. The slow time constant is τ_s = 5.5 ps ± 0.2 ps and the fast time constant is τ_f = 0.43 ps ± 0.02 ps.

The C_i^f coefficient relates directly to the population distribution for each mechanism. This coefficient can be calculated from the nascent populations using the equation,

$$C_i^f = \frac{\Sigma\left[P_{fast}(v,J,\Omega,\Lambda) \times B(v',J';v,J) \times Spec(v',J';v,J)\right]}{\Sigma\left[P_{obs}(v,J,\Omega,\Lambda) \times B(v',J';v,J) \times Spec(v',J';v,J)\right]}. \quad (5)$$

In this expression, the summation includes all the transitions that the probe laser encompasses; $B(v', J'; v, J)$ represents the Einstein B-coefficient for the designated transition; $P_{obs}(v, J, \Omega, \Lambda)$ is the experimentally determined nascent population distribution for OH; $P_{fast}(v, J, \Omega, \Lambda)$ is the population distribution for OH created through the fast mechanism; and $Spec(v', J'; v, J)$ is the power spectrum of the probe pulse at the excitation frequency. The difficult task is dividing $P_{obs}(v, J, \Omega, \Lambda)$ into two components, $P_{obs}(v, J, \Omega, \Lambda) = P_{fast}(v, J, \Omega, \Lambda) + P_{slow}(v, J, \Omega, \Lambda)$.

An easy approach is to fit the observed population as the sum of two Boltzmann distributions and to identify $P_{hot}(v, J, \Omega, \Lambda)$ with the fast channel and $P_{cold}(v, J, \Omega, \Lambda)$ with the slow channel,

$$\frac{P_{obs}(v,J,\Omega,\Lambda)}{2J+1} = C_{hot} Exp\left(-\frac{E_{rot}}{kT_{hot}}\right) + (1 - C_{hot}) Exp\left(-\frac{E_{rot}}{kT_{cold}}\right) \qquad (6)$$

A least-squares fit of Eq. (6) to the v = 0 data gave, T_{hot} = 4,110 K ± 106 K, T_{cold} =156 K ± 7 K, and $(1 - C_{hot}) / C_{hot}$ = 3.5. For v = 1, the fit yielded T_{hot} =5,980 K ± 80 K, T_{cold} = 131 K ± 6 K, and $(1 - C_{hot}) / C_{hot}$ = 3.9. These fit values represent the data well as shown in Fig. 8. The values of $(1 - C_{hot}) / C_{hot}$ correspond to only 11 % of the OH being formed in the cold/slow channel, while 89 % is from the hot/fast channel. Applying $P_{hot}(v, J, \Omega, \Lambda)$ determined from the Boltzmann distribution to Eq. (5) produces the calculated C_i^f coefficients in Fig. 7 (square symbols). The calculated coefficients are significantly higher than those derived from the time-resolved data. Therefore, the simple identification $P_{hot}(v, J, \Omega, \Lambda)$ with the fast channel is not consistent with the data. Moreover, there is no general justification for products having Boltzmann distributions,[49] because the available energy is limited by the sum of the enthalpy for the reaction $CH_4 + O_3 \rightarrow CH_3 + OH + O_2$ and the energy of the photolysis photon.

Another way to divide the observed population distribution into the components that Eq. (5) implies is to carry out a surprisal analysis.[50] The rotational surprisal, $I(v, J, \Omega, \Lambda)$, defined as

$$I(v,J,\Omega,\Lambda) = -ln\left(\frac{P_{obs}(v,J,\Omega,\Lambda)}{P_o(v,J,\Omega,\Lambda)}\right) \qquad (7)$$

is calculated as a function of rotational energy. The two reaction mechanisms may have characteristic and distinctly different linear surprisals, aiding in the deconvolution of $P_{obs}(v, J, \Omega, \Lambda)$ into $P_{slow}(v, J, \Omega, \Lambda)$ and $P_{fast}(v, J, \Omega, \Lambda)$. To complete this analysis, the rovibrational prior distribution, $P_o(v, J, \Omega, \Lambda)$, must be computed. In our calculation of the prior, the production of all quantum states was taken as equally probable, subject only to energy conservation. This distribution would be expected

in the absence of any dynamical constraints. The Whitten-Rabinowitz state count was used for the vibrational states and a classical partition function for the CH_3 fragment.[51,52] An exact count was used for the hydroxyl fragment. The prior was then taken as the product of the degeneracy of internal states of both fragments and the translational state density divided by total state density at the energy available to the reaction.[53,54,55] The prior was calculated for each OH(v, J, Ω, Λ) level individually. The energy available in the reaction was taken to be the sum of the enthalpy of the reaction $CH_4 + O(^1D_2) \rightarrow CH_3 + OH$ (15,240 cm^{-1}) and the average translational energy in the center-of-mass frame (1515 cm^{-1}). This number is correct for a free reaction, and using it here assumes that the O_2 generated in the cluster receives the same energy as in the photodissociation of isolated, gaseous O_3. The sum over rotational states, $\Sigma P_o(v, J, \Omega, \Lambda)$ was normalized to $\Sigma P_{obs}(v=0,1; J, \Omega, \Lambda)$ for each vibrational level.

Figure 9 shows the rotational surprisal for OH(v=0,1) plotted versus the fraction of non-vibrational energy in rotation, $g_r = f_r/(1 - f_v)$, where f_r and f_v is the fraction of the total available energy as rotation and vibration, respectively. If $P_{obs}(v, J, \Omega, \Lambda)$ were statistical, the data would fall on a line with a slope of zero. The distribution at low g_r is much colder than the prior distribution, while the distribution at high g_r is hotter than the prior distribution. The surprisal was fit with the equation,

$$I(v,J,\Omega,\Lambda) = -ln\left[\frac{P_{cold}(v,J,\Omega,\Lambda)+P_{hot}(v,J,\Omega,\Lambda)}{P_o(v,J,\Omega,\Lambda)}\right] = -ln\left[b_{cold}Exp(m_{cold}g_r)+b_{hot}Exp(m_{hot}g_r)\right] \quad (8)$$

Least squares fits gave m_{cold} = -128 ± 13, m_{hot} = 2.6 ± 0.2, b_{cold} = 2.53 ± 0.38, and b_{hot} = 0.56 ± 0.03 for v=0; for v=1, values m_{cold} = -138 ± 18, m_{hot} = 4.0 ± 0.3, b_{cold} = 3.00 ± 0.61, and b_{hot} = 0.51 ± 0.03 were obtained. The data for v=0 and 1 are well fit by the sum of two linear surprisals, as shown by the dashed lines in Fig. 9. Two population distributions, $P_{hot}(v, J, \Omega, \Lambda)$ and $P_{cold}(v, J, \Omega, \Lambda)$, can be deduced from the surprisal fits. Applying $P_{hot}(v, J, \Omega, \Lambda)$ determined from the surprisals to Eq. (5) produces the calculated coefficients in Fig 6 (triangle symbols). The calculated coefficients are significantly higher than the C_i^f deduced from the time-resolved data. Again, the simple identification $P_{hot}(v, J, \Omega, \Lambda)$ with the fast channel is inconsistent with the data.

It appears that the time-resolved and state-resolved data cannot be simultaneously fit with a two-mechanism model. The $P_{obs}(v, J, \Omega, \Lambda)$ data can be decomposed into two unique components. The time-resolved data are quite well fit by the sum of two exponential OH rise times. However, the amplitudes of fast and slow components do not match the amplitudes of the hot and cold distributions. There are other flaws in the two-state fits. The residuals in Fig. 6 show that some of the rise times are not exactly

fit by two exponentials. In the surprisal analysis of $P_{obs}(v, J, \Omega, \Lambda)$, the values of m_{hot} and m_{cold} necessary to fit the data are contrary to what one would expect. One might reasonably assume that the slow OH is formed from a CH_3OH^* intermediate in which energy has randomized, while the fast OH is not. If one identifies the latter with the hot surprisal, then one must identify the statistical component with the cold surprisal. However, it is difficult to see why a statistical dissociation should give a surprisal slope of -128, grossly different from the statistical expectation of m=0.

The observation of a component with a slow rise time of ≈5 ps suggests that one of the reactive channels produces OH through an CH_3OH^* intermediate in which the energy is randomized. An RRKM calculation in Appendix B also supports the idea that 5.4 ps is the lifetime expected for CH_3OH^* at the energy available in the $CH_4 \bullet O_3$ photolysis experiments. One might expect the rovibrational energy distribution of the products generated by this channel would be the prior distribution calculated above. Studying the distribution of product rovibrational energy following infrared multiphoton photodissociation (IRMPD) of CH_3OH can provide some insight into this assumption. This is considered in Appendix B, which analyses data from this laboratory and two other groups for OH population distribution and the tranlational energy released. The conclusion reached from these data is that the OH product does have an internal energy distribution similar to that of the prior distribution. In other words, for the levels of excitation in the IRMPD experiments, OH from energy-randomized CH_3OH^* is characterized by a zero-slope on a surprisal plot.

Because the two-channel model failed to characterize the data consistently, a three-channel fit was attempted. Each ultrafast data set was optimized to the following functional form,

$$LIF(t_d) = X(t_d) \otimes \left[C_i^f \times OH_f(t_d) + C_i^i \times OH_i(t_d) + C_i^s \times OH_s(t_d) \right] \qquad (9)$$

where as before $X(t_d)$ is the measured photolysis-probe cross-correlation, C_i^f, C_i^i, and C_i^s are the fraction of the fast, intermediate, and slow components, which were normalized such that $C_i^f + C_i^i + C_i^s = 1$. Each channel was assumed to have a single, exponential rise. The six data sets were fit simultaneously by varying fifteen parameters: twelve fractional coefficients and three time constants. The optimize values for C_i^f, C_i^i, and C_i^s are presented in Fig. 10 (open symbols). The three time constants determined are $\tau_{fast} \approx 200$ fs ± 70 fs, $\tau_{inter} \approx 500$ fs ± 50 fs, and $\tau_{slow} \approx 5.4$ ps ± 0.3 ps. Figures 4 and 5 show the fits to the data. The residuals displayed in Fig. 6 show that the three-channel model gives a slightly better fit than the two-state model to the fast rise of the 307.3 nm and 311.9 nm data and a much better fit to the 308.8 nm data, though the fits at 313.3 nm and 316.5 nm are not significantly

improved. Fitting to four rate constants did not significantly reduce χ^2 and gave markedly increased uncertainties in the best-fit parameters.

The rotational surprisals were also fit to three distributions. On the weight of the IRMPD data and the time constant, one will be taken to be the statistical prior, which is to say the slope of its surpisal is zero. Of the other two, one will assumed to be hotter and the other colder than the prior distribution. The surprisals were fit using the equation

$$I(v,J,\Omega,\Lambda) = ln\left[b_{cold}\,Exp\left(m_{cold}\,g_r\right) + b_{stat}\,Exp\left(m_{stat}\,g_r\right) + b_{hot}\,Exp\left(m_{hot}\,g_r\right)\right] \qquad (10)$$

With $m_{stat} \equiv 0$, a least squares fit to the v=0 data in Fig. 9 gave m_{cold} = -129 ± 13, m_{hot} = 6.0 ± 0.5, b_{cold} = 3.16 ± 0.35, b_{hot} = 0.07 ± 0.02, and b_{stat} = 0.67 ± 0.03. With these values, the population in each of the three distributions may be calculated, giving 12 % of the OH(v=0) created cold, 21 % hot, and 67 % statistical. The data for the v=1 level were fit by assuming the statistical channel has the calculated prior value for the v=1/v=0 population (21%), therefore, b_{stat} was set to a fixed value of 0.15. The least squares fit to the v=1 data gave m_{cold} = -131 ± 18, m_{hot} = 4.7 ± 0.3, b_{cold} = 3.16 ± 0.51, and b_{hot} = 0.38 ± 0.02. This fit gave 11 % cold, 74 % hot, and 15 % statistical for v=1. The solid lines in Fig. 9 show these fits to the surprisals. As expected, the surprisal data are slightly better fit by the three-distribution model than by the two-distribution model. As described for the two-mechanism simulation, coefficients $C_i^{f/i/s}$ for the six probe wavelengths may be calculated from the $P_{obs}(v, J, \Omega, \Lambda)$ distributions deduced from the surprisal analysis. Figure 10 compares the $C_i^{f/i/s}$ for the three mechanisms that fit the time-resolved data (open symbols) to the $C_i^{f/i/s}$ calculated from the state-resolved data (closed symbols). For all wavelengths, there is close agreement, if the following identification is made: We associate the OH formed fastest with OH formed in the lowest N levels [τ_{fast} ≈0.2 ps and $P_{cold}(v, J, \Omega, \Lambda)$], the OH formed at the intermediate rate with the hot distribution [τ_{inter} ≈0.5 ps and $P_{hot}(v, J, \Omega, \Lambda)$], and the OH formed slowest with the statistical channel [τ_{slow} ≈5.4 ps and $P_{stat}(v, J, \Omega, \Lambda)$]. Therefore, this three-mechanism model is consistent with the data. However the three rovibrational distributions are not unique, because there are other distributions with nonlinear surprisals which also fit the data. We note that improved agreement between the coefficients calculated from time- and state-resolved data can be achieved by varying the fitting parameters slightly from their best fit values.

The curves in Fig. 11 show the fraction of cold, statistical, and hot product as a function of internal energy calculated from the three-distribution fit parameters. One sees that the cold distribution only contributes significantly to the four, lowest rotational levels. The statistical distribution contributes

to the majority of the probed levels, at least for v=0, while the hot distribution contributes primarily to OH with an internal energy ≥4000 cm^{-1}. Though we have no data only for v=0 and v=1, this model predicts that the statistical mechanism makes a negligible contribution to vibrational levels ≥2. If one desires an analytic expression for any of the three individual rovibrational distributions, one may use Eq. 10, after suitable rearrangement, and its best-fit parameters, with Eq. 6 and its best-fit parameters to represent $P_{obs}(v, J, \Omega, \Lambda)$.

Mechanism Assignments. The long time constant is almost surely the dissociation of a methanol after complete IVR according to statistical theory, such as the Rice-Ramsburger-Kassel-Marcus (RRKM) theory.[56] In Appendix B, a RRKM lifetime calculation, consonant with thermal rate coefficients and assuming reasonable values for the CH_3OH^* transition state, fit both the time scale (≈10 ns) for dissociation in the IRMPD experiments and the time scale (≈5 ps) for dissociation at the 16,700 cm^{-1} energy in the cluster photolysis experiments.. This supports the statistical assignment, because one expects the RRKM rate to scale correctly with internal energy, even though exact agreement is usually achieved only if the transition state is selected to fit a particular microcanonical rate. Statistical adiabatic channel model calculations[57] predict lifetimes of 10 ps for the reaction of thermal $CH_4 + O(^1D_2) \rightarrow CH_3OH^*$ at an energy 1300 cm^{-1} less than our hot $O(^1D_2)$ experiments, and 1.6 ps for $O(^1D_2)$ atoms from N_2O photodissociation at 193 nm, providing 7700 cm^{-1} more available energy than in our experiments. These estimates of the lifetime of CH_3OH^* are also in agreement with the value of 5.4 ps observed for the slow component, which is also the slowest rise time measured. No intermediate should dissociate more slowly than that following complete IVR. If IVR is complete within picoseconds—and the contrary would be unexpected at this energy[58]—the longest formation time is, by default, the statistical lifetime. These observations argue for identifying the slow channel with the statistical dissociation of a CH_3OH^* intermediate.

The intermediate formation time of 0.5 ps is ascribed to dissociation a CH_4O^* intermediate before IVR and associated with the high-J fraction of OH arising from this reaction. This component accounts for about 21% of the population in v=0, 74% for v=1, and presumably most of the population in v=2 – v=4. At least three observations bolster this assignment. First, evidence overwhelmingly suggests that $O(^1D_2)$ insertion is the predominant reaction mechanism,[3,4,5,6,21,59,60,61] pointing to non-statistical dissociation of CH_4O^*. Second, and related, a 0.5 ps rise time seems too long to be a stripping of a H atom by fast O (forward scattering limit) or a collinear abstraction by fast O (backward scattering limit). The attacking oxygen atom initially moves with an average speed of ≈2.1 nm ps^{-1} and hence

would travel the 0.3 nm – 0.4 nm necessary for a simple stripping reaction in much less than 0.5 ps. The product OH would presumably gain additional translational energy from the reaction exothermicity, which, in the absence of complex formation, would further decrease the estimated time for a stripping reaction. Last, the OH product is too hot to be the statistical channel. Together, these observations suggest dissociation through a CH_4O^* intermediate before IVR

The most tenuous part of the present data analysis is the very fast time (0.2 ps) associated with OH in low-J states. This OH accounts for about 11 % of the population in both v=0 and v=1 levels. Fast OH could be formed by O moving perpendicular to a C–H bond and stripping off a H atom at impact parameters sufficiently large to avoid being trapped in the CH_3OH well. Such trajectories presumably would give rise to forward-scattered OH in high, rather than low, rotational states. Collinear attack followed by prompt back scattered OH could give rise to OH in the low-J levels that seem to be correlated with the shortest time constant. The saddle point on the $O(^1D_2)$ potential surface[15] shows such a collinear C–H–O reaction. Some abstraction component seems consistent with the Doppler spectroscopy results[7,8,9,10,11] which show a slight preference for backward scattering for the OH(v=0, J=5 and 8). Our decomposition shows that the prompt component contributes mostly to the four lowest f_1 rotational states and predicts that these states would show pronounced backward scattering.

An alternative explanation for the fast OH in low-J, f_1 levels is reaction of $O(^3P_j)$ formed in about 10 % yield in O_3 photolysis with 267 nm light.[62] This possibility cannot be excluded. On the other hand, low-J, f_1 OH was also preferentially populated in the photolysis of the $CH_4 \bullet N_2O$ cluster,[27] and no $O(^3P_j)$ atoms are formed directly in N_2O photolysis. The $O(^3P_j)$ may also be involved through $O(^1D_2)/O(^3P_j)$ curve crossing in the entrance channel. However, *ab inito* calculations of the singlet surfaces allow for abstraction trajectories, so although such crossing may occur, it may not be required to explain the $CH_4 \bullet N_2O$ or $CH_4 \bullet O_3$ results.[15] This alternate explanation is discussed in greater detail in Appendix A, where it is shown that the present three-mechanism model is consistent with data from Doppler, beam scattering, chemical kinetic, chemical quenching, and product state experiments, as well as recent theory.

Limitations of the present experiment. In these experiments, the appearance rate for most of the product states has not been measured. The free reaction, and presumably the cluster reaction, between CH_4 and $O(^1D_2)$ produces about half of the OH in vibrational levels v>1, with v=2 the most probable and levels up to v=4 populated.[6] The experiment reported here investigated no levels above

v=1. Moreover, the highest rotational states even for these two vibrational states were not monitored, because of the autodissociation of OH(A). Therefore, the conclusions drawn here are based on probing somewhat less than half the OH product from the reaction. In our preliminary experiments,[23] only OH(v=0, J) formed predominantly through the statistical channel, was probed. As a result, we failed to discover the fast components discussed here. This earlier failure highlights the desirability of obtaining more comprehensive data.

Another limitation of the data presented here is that each appearance curve represents an complicated superposition of many rovibrational states, because of the inherently broad spectrum of short pulses compared to the spacing of individual OH transitions. An absorption experiment could allow measurement of the appearance of individual OH(v, J, Ω, Λ) states. Following photolysis, spectrally broad ultrafast pulses could probe the OH, and a spectrometer could disperse the transmitted light onto a multichannel detector. With this approach, the experimental time resolution is limited by the laser pulse duration, the experimental spectral resolution by the spectrometer, and the observed linewidths by the sample dephasing time.[63] This approach might also permit probing the OH close to the transition state,[64,65] where the OH*(X)* and OH*(A)* potentials are perturbed by the CH_3 or O_2 fragments. Such information, combined with sub-Doppler spectra of individual rovibrational states, would yield a more complete picture of the dynamics of this reaction. Although three rise times adequately represented our LIF data within the present signal-to-noise, the idea that there are three distinct OH formation mechanisms, each characterized by a distinct distribution, is presumably overly simple. In the absence of supporting theory, no particular reason exists to believe that all reactive trajectories group neatly into separate and characteristic types. In the absorption experiment idealized above, one can imagine that each OH(v, J, Ω, Λ) might have different and complex time dependence for the absorption spectra on short time scales, with our LIF results representing an ensemble average.

Throughout this paper we compared free and cluster reaction results with the unstated assumption that the reaction mechanisms are similar. However it is an extremely important question to what extent the trajectories of $O(^1D_2)$ attacking CH_4 in the cluster resemble the trajectories in the free, gas phase reaction. We observed that the OH v=1/v=0 ratio for the cluster was the same as for the free reaction and that the rotational state distributions were generally similar.[28] These observations suggest, but do not prove, that reaction mechanisms in the cluster are similar to those for the free reaction. The CH_4•O_3 cluster geometry, which has not been reported, could have a significant impact on the observed dynamics, and a potential energy surface for this van der Waals complex would be helpful. The

dissociation of gaseous O_3 has been studied and the dynamics of forming $O(^1D_2)$ and O_2 are fairly well understood. Presumably, complexation does not significantly alter this dissociation process. There is almost complete dissociation within 60 fs – 80 fs.[66,67,68] The average asymptotic velocity of the $O(^1D_2)$ is ≈2.1 nm ps^{-1},[62] directed along the initial O_2-O bond,[69] and the O_2 travels ≈1.1 nm ps^{-1}. The O_2 molecule should not alter the long-lived CH_3OH^* dissociation, because the diatom would be on average ≈6 nm away from the dissociating methanol. Our RRKM calculations and calculations of the statistical prior energy distributions for the OH and CH_3 products assumed the energetics of the free reaction, i.e., the energy carried by the O_2 molecule was assumed to be unaffected by the complex, an idea which is supported by the similarity between the OH energy distributions for free and cluster reactions.

V. Summary

The mechanism of the reaction $CH_4(\tilde{X}\,^1A_1) + O(^1D_2) \rightarrow CH_3(\tilde{X}\,^2A_2'') + OH(X\,^2\Pi)$ was investigated by state-resolved and ultrafast, time-resolved experiments on the $CH_4 \bullet O_3$ van der Waals complex in which O_3 was photolyzed to produce $O(^1D_2)$. Our experiments only probed OH in the v=0 and v=1 levels, which accounts for somewhat less than half of the total OH formed. Both fast (<1 ps) and slow (≈5 ps) rise times in the fluorescence signal were observed, and the ratio of fast-to-slow signal varied as the probe wavelength was changed. The distribution of OH states, $P_{obs}(v, J, \Omega, \Lambda)$, is well represented by the sum of two Boltzmann distributions with different rotational temperatures. The $P_{obs}(v, J, \Omega, \Lambda)$ data and the time-resolved data were fit simultaneously using the idea that different formation times represent different reaction mechanisms, and that each reaction mechanism gives rise to a characteristic rovibrational distribution. This required that data be decomposed into three formation rates and rovibrational distributions. The $P_{obs}(v, J, \Omega, \Lambda)$ was decomposed into three components with linear surprisals, assuming that a statistical mechanism gave OH distributed according to the statistical prior. The three component model consistently fit both state- and time-resolved data. The time-resolved data were fit with times $\tau_{fast} \approx 0.2$ ps, $\tau_{inter} \approx 0.5$ ps and $\tau_{slow} \approx 5.4$ ps. The slowest mechanism was attributed to dissociation of a CH_3OH^* intermediate at a rate predicted by statistical theory. Dissociation of a CH_4O^* intermediate before complete energy randomization produces OH more quickly (τ_{inter}) and with more rovibrational energy than the slow mechanism. The third mechanism produces OH promptly with a little rotational excitation, indicative of a collinear abstraction mechanism. The three derived rovibrational distributions, which are model dependent and therefore not unique, correspond to fast, intermediate, and statistical components of 12 %, 21 %, and 67 % of population in OH(v=0) and 11 %, 74 %, and 15 % in OH(v=1). Presumably dissociation of the CH_4O^* intermediate produces most of the

population in higher vibrational levels not probed in our experiments. This model helps to reconcile a variety of data from previous experiments. To support the assumption that of dissociation through a methanol intermediate after IVR, the distribution of energy in OH from the CO_2 laser-induced, infrared-multiphoton dissociation (IRMPD) was analyzed.

Acknowledgments

C. Cameron Miller acknowledges the receipt of an NIST/NRC Postdoctoral Fellowship. The IRMPD data were measured with the help of David S. King and Joseph A. Blazy.

Appendix A: Comparison of the CH_4•O_3 Results to Previous Studies of Reactive Collisions Between CH_4 and O.

As highlighted in the introduction, the literature contains a wealth of available information concerning the thermodynamic, chemical kinetic, and molecular dynamics studies of the reaction between $CH_4 + O(^1D_2)$. In this appendix, we critically review this literature as it pertains to our results. The objective of this comparison is to look for evidence in the literature that will bolster the mechanistic assignment of this paper and to help unify this sizable literature into a comprehensive understanding of the dynamics of the title reaction.

Matrix and Chemical Timing Experiments. Much of our intuition about the reactions between atomic oxygen and hydrocarbons is derived from the early work of Cvetanvic and coworkers[61] and Demore and coworkers.[3,4,5] Cvetanvic and coworkers[61] proposed three distinct mechanism: Insertion and fragmentation, abstraction to form OH, and elimination of molecular hydrogen. In experiments carried out in a liquid argon matrix aimed at further elucidating the role of the these proposed mechanism, Demore and Raper[4] identified three products for the reaction with methane,

$$\begin{aligned} CH_4 + O(^1D_2) &\rightarrow \quad CH_3OH \\ &\rightarrow \quad H_2CO + H_2 \\ &\rightarrow \quad CH_3 + OH. \end{aligned}$$

The fraction of reactants going into each of these three channels was, respectively, 53 %, 7 %, and 40 %. From this early work, Demore speculated that a CH_3OH^* might be common to all these reaction paths. However, subsequent studies of the free reaction in the gas phase reaction at room temperature lead Lin and Demore[3] to conclude that about half of the total CH_3 and OH produced passed through a CH_3OH^* intermediate, which they estimated to have a lifetime of about 0.8 ps. Production of the other half was attributed to a different prompt mechanism. The production of methyl and hydroxyl radicals at high pressures and even in liquid argon is frequently cited as evidence for an abstraction mechanism that does not involve a methanol-like intermediate. The results of Demore and coworkers pose two questions. First, is the 0.8 ps consistent with the lifetimes measured in our experiments? Second, does production of methyl and hydroxyl radicals even in liquid argon demand an abstraction channel?

To answer the first question, it is important to understand how the 0.8 ps lifetime was determined. The $O(^1D_2)$ was generated by 184.9 nm photolysis of nitrous oxide, and the translational energy was neither nascent nor fully thermalized. This generation process gave ≈20 % uncertainty in the total available energy. The value of 0.8 ps was calculated from the slope-to-intercept ratio (the intercept

value being an extrapolation from finite to zero pressures) of a plot of the ratio of the concentration of methanol to the pressure of the cooling gas as a function of methane concentration. While our experiments probe a limited subset of the total product states, the 0.8 ps value is nevertheless similar to the population-weighted average of the rise times that we measured directly. Olzmann[57] has also note that Lin and Demore used a strong-collision model in analyzing the chemical timing data, and if one assumes that the collisional cooling rate is different than gas kinetic, a somewhat different lifetime can be extracted from these experiments. Given the experimental uncertainties and differences between the experiments of Demore and coworkers and the data presented here, we believe that the two lifetime measurements are in remarkable agreement.

To answer whether formation of CH_3 and OH from CH_4 + $O(^1D_2)$ in liquid Ar requires an abstraction channel, one may compare the vibrational relaxation time of CH_3OH^* in liquid argon to the dissociation time of CH_3OH^*. The collisional stabilization time, τ_{vr}, can be estimated as

$$\tau_{vr}^{-1} = k_{vr}\rho g(r). \qquad \text{(A1)}$$

In this expression, k_{vr} represents the vibrational relaxation rate constant of CH_3OH^* in liquid argon at a temperature of 87 K, ρ is the density of the liquid argon, and $g(r)$ is the radial distribution function evaluated at the Lennard-Jones diameter.[70] The exact value for k_{vr} is not known, but it is likely to be slightly less than the gas kinetic rate, and we assume it to be $\approx 10^{-10}$ cm^3 s^{-1}. The matrix density is $\approx 2.3 \times 10^{22}$ cm^{-3}. The value of the radial distribution is also unknown, though in general it lies between 1 and 3, and we will take a value of 2. Using these numbers in the Eq. B1 gives a $\tau_{vr} \approx 0.2$ ps. If we take the dissociation time, τ, to be 0.5 ps (the dissociation time we have assigned to the incomplete IVR mechanism), then the probability of the intermediate dissociating prior to vibrational relaxation is $1 - exp(-\tau_{vr}/\tau) \approx 0.33$. That is, one third of the CH_3OH^* would have dissociated into CH_3 and OH prior to stabilization of CH_3OH^*. This number lies very close to 40 % reported for the matrix reaction. This estimate suggests that the collision stabilization of CH_3OH^*, even in liquid argon, is unlikely to be much faster than the rate of OH formation. Therefore, observation of OH does not necessarily suggest an abstraction mechanism against an insertion/elimination mechanism. It should be noted that photolysis of O_3/CH_4 mixtures in a solid argon matrix at 20 K reportedly gives only CH_3OH.[71] This may be because IVR is faster in solid than liquid Ar, or more likely, that the fragments are trapped so that geminate recombination occurs.

State-Resolved OH(v, J, Ω, Λ) Measurements. In his pioneering studies of this reaction, Luntz[60] photolyzed ozone at 266 nm in a $Ar/O_3/CH_4$ mixture and probed OH(v=0,1). The experiments

were carried out at a density of 6×10^{16} cm^{-3} and a photolysis/probe time delay of 0.5 μs, presumably ensuring that the hot oxygen atoms formed in the photolysis were thermalized prior to reaction. As a result of this thermalization, the $O(^1D_2)$ carried ≈1200 cm^{-1} less available energy; moreover, the $O(^3P_j)$ atoms lacked sufficient translational energy to surmount the barrier for reaction. However, the long photolysis/probe delay and the relatively high pressures opened the possibility of collisions that would alter the nascent distribution, though Luntz maintained that the distributions were close to nascent. Luntz reported that v=0 and v=1 were comparably populated and had similar rotational state distributions. The f_1 and f_2 spin-orbit states were equally populated, and the Λ-doublet ratio increased from unity at low-N to ≈1.7 at N=19. A surprisal analysis was done for the rotational distribution. Luntz decomposed this surprisal into two regions. Levels for N>6 were well fit by a line of slope ≈6.5, whereas states for N <6 were much colder, and deviated greatly from a linear surprisal. From the data in Luntz's Fig. 2, the cold component can be estimated to be ≈7 % of the total population. The $P_{obs}(v, J, \Omega, \Lambda)$ peaks at $g_r \approx 0.3$. Luntz attributed the population characterized by the linear surprisal as product from a CH_3OH^* intermediate before complete IVR. The minor, cold OH was from an in-line collision at low impact parameter giving rotationally unexcited product. Our analysis of the data from these experiments is consonant with his interpretation of the distribution for high-N. However, we believe there is a significant contribution from a statistical channel which contributes to OH at both intermediate- and low-N, which would be identified if our three-mechanism model were used to analyze Luntz's data.

In a similar set of experiments, Park and Wiesenfeld (PW)[6] probed OH(v=0,1,2,3,4) following 248 nm photolysis of ozone in a $Ne/CH_4/O_3$ mixture. A density of 5×10^{15} cm^{-3} and a delay time of 0.2 μs were used, which should make the $P_{obs}(v, J, \Omega, \Lambda)$ close to nascent, though the cooling of the hot $O(^3P_j)$ before a reactive collision would be incomplete. The fractional population in vibrational levels v=0 – 4 was reported to be 0.25, 0.25, 0.33, 0.12, and 0.05, respectively. These vibrational populations are in fair agreement with those from an infrared chemiluminescence study[72] (which could not probe v=0) and a LIF study that probed rotationally relaxed OH(v=0,1,2).[73] PW found that a temperature of ≈7000 K characterizes $P_{obs}(v=0, J, \Omega, \Lambda)$ well for products within the range 1000 cm^{-1} – 10,000 cm^{-1}. At lower-N, a second, almost thermal component was observed, though PW did not give a characteristic temperature. They reported near-equal population of the two spin-orbit states and an average A′/A″ ratio of ≈1.6, which increased with N. Both the v=0 and v=1 surprisals were linear between g_r of 0.17 and 0.7, with a slope of ≈5.5. The surprisal of the v=0 data, shown in Fig. 12 of their paper, is linear with a

slope near zero for rotational levels $g_r < 0.17$. PW interpret the high-N population producing the linear surprisal as arising from insertion and elimination before energy randomization. The colder OH was ascribed to dissociation of CH_3OH^* after energy randomization. PW reported that fraction of the rotational population arising from this second channel to be 18 % and 6 % for v=0 and v=1, respectively. It appears the PW v=0 data for states with <3000 cm!1 lie very close to a linear surprisal with a slope m =0. It is likely that if the PW data were analyzed by the three state model above (one channel to be characterized by an unconstrained prior), a statistical channel greater than 18% would be deduced.

Wada and Obi (WO) have reported $P_{obs}(v=0,1; J, \Omega, \Lambda)$ of OH from $CH_4 + O(^1D_2)$ both for the free reaction and for the $N_2O \bullet CH_4$ cluster.[27] Photolysis of N_2O at 193 nm produced the $O(^1D_2)$ with an average total energy for the reaction of about 18,400 cm^{-1}. For the free reaction, a v=1/v=0 ratio of 1.1 was measured. For both v=0 and v=1 the high-N levels are characterized by a temperature of ≈13,000 K and for the low-N states a temperature of ≈1000 K. WO found the average f_1/f_2 ratio to be 1.1 for v=0 and v=1. The average value of A′/A″ was 1.9 for v=0 and 1.3 for v=1. For the cluster reaction, they found the same v=1/v=0 ratio, comparable rotational distributions and A′/A″ ratios. Notably, the f_1/f_2 ratio at low N was larger for the cluster than for the free reaction and resembles the $CH_4 \bullet O_3$ cluster data in Fig. 8. The high-N cluster data gave a linear surprisal, with a slope of 6.9 for both v=0 and v=1. They deduce the cold, low-N population to be 24% of the total for v=0 and 7% for v=1 for the cluster, and 16 % and 5 % for the free reaction. They assigned the colder OH to the dissociation of CH_3OH^* after complete energy redistribution and the hotter, high-N to insertion of $O(^1D_2)$, followed by dissociation prior to complete IVR.

The WO fits to their $P_{obs}(v, J, \Omega, \Lambda)$ results are quantitatively different from our results, although we believe that different approaches to data analysis account for some of the apparent discrepancy. WO give much hotter values for the rotational temperature at high-N (13,000 K compared to our result of 4100 K for v=0 and 6000 K for v=1). The differences seem greater than can be accounted for by the 11% higher available energy in the $CH_4 \bullet N_2O$ photolysis. However, while the WO data for the v=1 level has a great deal of scatter, it does appears to overlap our v=1 $P_{obs}(v, J, \Omega, \Lambda)$ plots almost exactly. Perhaps some difference in the temperature determinations accounts for these apparent differences, or perhaps the derived values overlap within the associated uncertainties. The value of the surprisal slope of 6.9 may be compared to our value of 5.5 in our three-state fit. It appears from WO's Fig. 6 that much of the data for $g_r < 0.2$ could be fit by a linear surprisal of slope zero. It is likely that if

the WO data were analyzed using a three state model, a statistical channel greater than 24% for v=0 and 5% for v=1 would be deduced, bringing their conclusions closer to ours.

Naaman and coworkers[74,75] measured $P_{obs}(v, J, \Omega, \Lambda)$ after initiating the reaction by 266 nm photolysis of O_3 in a crossed beam experiment. The rotational distribution for v=0 and v=1 were reported for N < 14. For v=0, these distributions are hotter than our cluster results and cooler than those of PW. Naaman *et al.* report f_1/f_2 of ≈2.4 and ≈1.3 for the low-N levels of v=0 and v=1, respectively; other rotational levels appear to have ratios near unity. The authors stated that there is a slight preference for the f_1 spin-orbit state after correcting for the *2J+1 = N/N+1* statistical weight. Naaman *et al.* report that the A′/A″ ratio for OH(v=1) increases from ≈2 to ≈10 between N=1–13. This unusually large propensity of the A′ state was attributed to the cold temperatures of the beam. A similar propensity has not been observed in reactions initiated in van der Waals clusters, where one might reasonably presume the rotational temperature of reactants to be comparable to those in a crossed beam experiment. The OH velocity distribution was also measured in the crossed-beam experiments and reported to have an average value of $\approx 6\times10^5$ cm s^{-1}. Because this value would correspond to a total translational energy release to both fragments of about 60,000 cm^{-1}, as compared to ≈ 22,100 cm^{-1} available, we presume it to be incorrect. In any event, the rotational distribution at low-N, spin-orbit ratio, Λ-doublet ratio, and velocity distribution reported for these crossed beam experiments are quite different from the results reported by Luntz,[60] Park and Wiesenfeld,[6] Wada and Obi,[27] and our laboratory.[28] Indeed, there is a strong congruence in this latter group of experiments. The surprising uniqueness in the data reported by Namaan and coworkers perhaps suggests that there are not-yet-understood differences between the data from the molecular beam environment and the cluster *and* cell environments.

Doppler Spectroscopy. Simons and colleagues have studied the free reaction between $CH_4 + O(^1D_2)$ using Doppler spectroscopy.[7,8,9,10,11] These investigations probed OH(v=0, N=5,8,19) and the very minor product OH(4, 8). The $O(^1D_2)$ in the Doppler experiments was from photolysis of N_2O at 193 nm and, as noted above, the reaction had substantially more translational energy than experiments using ozone photolysis. Nevertheless, this is still small compared to the reaction enthalpy and probably changes the lifetime of the statistical channel only slightly, though it is difficult to assess how the changed collision energy might alter the lifetime of the non-statistical channels.

Two conclusions from these Doppler profiles pertain to our experiments. First, for OH(0, 5, f_1 , A′ and A″) and OH(0, 8, f_1, A′) Doppler profiles showed the average translational energy was about a quarter of the available energy (Cf. Fig. 1d, 2d, & 3d of Ref. 10). The observed fraction of

energy in translations compares well to 20 % prediction by our prior calculations described above. Second, the differential scattering cross sections deduced from the detailed shape of the Doppler profiles OH(0,19) showed backwards scattering, with the most probable center-of-mass scattering angle of 115° with a FWHM of 70°. Similarly, for OH(v=0, N=5,8) about a quarter to a third of the product was scattered backward in a 40° cone about the line-of-impact. Neither of these scattering patterns is what would be expected for a long-lived complex.

In the Doppler experiments "long-lived" means with respect to the rotational time of the complex forming the OH state being probed. To reconcile the asymmetry in the differential scattering cross sections to our earlier report of only long-lived statistical formation of OH(v=0), Simons and coworkers postulated a correlation between the impact parameter (the rotational period of the CH_3OH^* intermediate is inversely proportional to the impact parameter) and scattering angle. Indeed, such a correlation may be associated with distinct mechanisms we have identified. In light of our present findings, however, it is likely that at least two reaction mechanisms contribute to each of the OH(v=0, N), so the observed distribution would be a superposition of an asymmetrical scattering distribution from a short-lived component and a symmetric distribution from the statistical channel. Our deconvolution of the population distribution into three components allows us to estimate that for the OH(v=0, N=5,8) levels about 80 % of the population was from the statistical channel, and about 20 % from the intermediate channel (Cf. Fig 10), which is comparable to the 25 % – 30 % back-scattering deduced from Doppler profiles.

Theory. Arai, Kato and Koda have calculated potential energy surfaces for $CH_4/O(^1D)$, subject to some geometrical restrictions.[15] The minimum energy path for the reaction travels along a narrow valley, with the O atom collinearly approaching the C–H bond, to a saddle-point with a collinear C–H–O structure. At this saddle-point the C–H bond length (110 pm) is close to the CH_4 equilibrium value, and the OH bond length is 166 pm, as compared to 97 pm for OH(*X*). The electronic energy of the saddle-point is only slightly higher than the separated reactants. From this transition state, the minimum energy path leads directly to CH_3OH in its equilibrium geometry. The exit channel leading to CH_3 + OH is broad and extends nearly up to the saddle point. This observation lead Arai *et al*. to suggest that the reaction might proceed through abstraction-like trajectories directly from the saddle-point without ever passing through a methanol-like geometry. This type of abstraction mechanism is different from the abstract mechanism postulated by Luntz,[60] who conjectured that crossing from singlet

to triplet surface occurred in the entrance channel and that the abstraction reaction then proceeded on the $^3A'$ and $^3A''$ surfaces.

The Reaction of CH_4 + $O(^3P_j)$. Because ozone photolysis near 266 nm has a $O(^3P_j)$ quantum yield of ≈10 %,[62] the possibility of $O(^3P_j)$ reactions must be considered. A ≈3500 cm^{-1} barrier to the reaction of $O(^3P_j)$ with CH_4 exists so substantial energy is necessary to promote this slightly endothermic reaction (ΔH°_{0K} = 7.5 kJ mol^{-1} = 630 cm^{-1}).[2] The distribution of translational energy in the $O(^3P_j)$ generated by ozone photolysis is broad,[62] but most atoms carry enough translational energy to overcome the barrier. On average there is ≈ 6400 cm^{-1} of translational energy available in the $O(^3P_j)$-CH_4 cm frame, so OH states v ≤ 2 could be populated. To assess whether $O(^3P_j)$ reaction are contributing to the time-resolved measurements reported here, we turn to what is known about the free, bimolecular reaction between $O(^3P_j)$ and hydrocarbons.

One aspect of $O(^3P_j)$ reactions that has been well studied is the rovibrational energy distribution in the hydroxyl product. Andresen and Luntz (AL) studied several larger hydrocarbons,[76] but not methane, and found that the rotational distributions were very cold and peaked at the lowest rotational level, even for reactions with sufficient energy to populate up to OH(v=0, N=15). For these hydrocarbons, the ratio $f_1/f_2 \times (N/N+1)$ was between 1.5 and 2.0 for OH(v=0, N<5), with possibly a propensity for the higher values at the lowest rotational levels. In a more recent study, Sweeney, Watson, and McKendrick (SWM) measured $P_{obs}(v=0, J, \Omega, \Lambda)$ for the OH product in a low-pressure cell,[77] for reaction with methane, ethane, n-hexane, and benzene. They generated $O(^3P_j)$ by photolysis of NO_2 at 248 nm to study the reaction with methane. The translational energy distribution of the $O(^3P_j)$ generated is broad,[78] and the most-probable translational energy is ≈9990 cm^{-1}, giving about ≈4900 cm^{-1} of available energy in the CH_4–$O(^3P_j)$ frame. The rotational distributions for the larger hydrocarbons were hotter in these experiments in comparison to those of AL, though this difference could just reflect different collision energies. The spin-orbit ratios were similar to those measured in the crossed beam experiment. For methane, the rotational distribution may be roughly characterized by a temperature between 800 K – 1100 K. The OH(v=0, N=1–7, f_1) states were found to have an average rotational energy of 580 cm^{-1}, ≈12 % of the available energy. No OH(v=1) could be detected and the rotational-state averaged Λ-doublet ratio was reported to be unity. Regrettably, neither of these numbers were accompanied by uncertainties.

The current understanding of the dynamics of CH_4 + $O(^3P_j)$ → CH_3 + OH has benefited from extensive calculations of the potential. One of the first of these was a semiempirical potential that was

adjusted for best agreement between the measured and calculated rovibrational distribution.[76] This potential had a minimum energy path, with a high barrier, along the O–H–CH_3 co-ordinate and shallow curvature in the C–H–O angle. More rigorous, *ab initio* calculations of the O(^3P_j) potentials[79,80,81] have found the same general features. The barrier to reaction is some 3300 cm^{-1} to 3600 cm^{-1} high. The minimum-energy configuration atop this barrier is the collinear C–H–O geometry. At this transition state, however, a 20° bend of the C–H–O angle costs only ≈350 cm^{-1}, which makes this potential more like a funnel than a tunnel. Indeed, Gonzáles *et al.*[82] found that reactive trajectories with ≈5240 cm^{-1} of available energy had an average C–H–O angle of 142° and a FWHM of 45°.

It has often been suggested that the origin of the high f_1/f_2 ratio points to an adiabatic reaction co-ordinate, inasmuch as only specific O(^3P_j) spin states correlate to particular OH spin-orbit levels.[83] All four potentials associated with $\Omega = {}^3/_2$ (f_1) correlate with O(^3P_j) surfaces, while those from $\Omega = {}^1/_2$ (f_2) divide between ^{3}A surfaces which connect to O(^3P_j), and ^{1}A surfaces which do not. When the O(^3P_j) spin-state distribution is accounted for, strict adiabatic correlation gives a spin-orbit ratio larger than observed in either experiment. This lead SWM to conclude that a combination of angular moment mixing in the entrance channel and spin-orbit coupling in the exit channel is the best explanation for the observed f_1/f_2 ratio. Just as the rotational distribution is indeed cold, but is in fact warmer than the prior; so the spin-orbit ratio is larger than predicted by the prior, but less than expect for a strictly adiabatic reaction.

One is tempted to take the OH(v=0, low-N) preferential population of the f_1 spin-orbit state as evidence for reaction between O(^3P_j) and CH_4. The two Boltzmann fit to our data gave a OH(v=0, low-N) distribution characterized by ≈150 K, but based on the three-channel model, the average energy for OH(v=0, f_1) for the coldest distribution is 86 cm^{-1}, which is only 2 % of the available energy. In either case, the distribution is significantly colder than the SWM results[77,83] and the trajectory calculations of Gonzáles *et al.*[82] However, the energy available in both experiments is both uncertain and broad; this temperature difference could conceivably reflect different energetics. More importantly, we observe this preferential population of the f_1 level both in v=0 and v=1, and the fractional population attributed to the fast/cold mechanism is the same (≈11%) for both vibrational levels. This contrasts with the experiment and theoretical finding that reaction with O(^3P_j) gives little population in v>0. Another point worth noting is that in the CH_4•N_2O cluster experiments—but not in the cell experiments using N_2O—a high f_1/f_2 ratio for low-N was also observed, and O(^3P_j) is not produced in the photolysis of N_2O. Wada and Obi[27] ascribed the high f_1/f_2 ratio to crossing from O($^1D_2$) to O(^3P_j) in the entrance channel for the

reaction. WO conjectured that the preference was evident only in the cluster reaction because reactive collision in the cluster reactions occur preferentially at low impact parameters. In contrast, the large nuclear orbital angular momentum associated with a reaction at higher temperatures tends to dilute the effect of the selection rules associated with the electronic angular momentum. WO also maintained that the high-f_1 population was to be expected for low-N components generated through a long-lived CH_3OH^* intermediate, though this assertion was unproven.

For the data presented here, the preferential population of f_1 at low-N could be due to reaction of nascent $O(^3P_j)$ formed in the photolysis of ozone. Although the equal population of this fast and cold component is equal in v=0 and v=1 and the similar distribution from the $CH_4 \bullet N_2O$ cluster suggest to us that this is not the case, this possibility cannot be eliminated. Another explanation is that entrance channel $^1D_2 / {}^3P_j$ curve crossing leads to an abstraction on the $O(^3P_j)$ potential, though we have no direct evidence for this alternative. It is also possible for both $CH_4 \bullet N_2O$ and $CH_4 \bullet O_3$ cluster experiments that the unusually large population in low-N f_1 states is an effect unique to the cluster, perhaps involving the adjacent N_2 or O_2 molecule or an orientation effect of the reactants in the cluster.

Other Channels. Although formation of CH_3 + OH is the primary channel in the bimolecular reaction between CH_4 + $O(^1D_2)$, it is not the only channel. The reported contributions of the various channels have varied greatly. For example, estimates of the contribution of the principal channel have spanned 69 % – 96 %. Lee and coworkers[19,20,84] recently critically reviewed of the work of Hack and Theismann,[21] Brownsword *et al.*,[16] Satyapal *et al.*,[18] and their own crossed-beam experiments and recommend the branching ratios listed below, which are given along with the standard enthalpies of reaction at 0 K.

$CH_4 + O(^1D_2)$	$\rightarrow CH_3 + OH$	69 %	-182 kJ mol^{-1}
	$\rightarrow CH_2OH + H$		-165 kJ mol^{-1}
	or	23%	
	$\rightarrow CH_3O + H$		-129 kJ mol^{-1}
	$\rightarrow H_2CO + H_2$		-482 kJ mol^{-1}
	or	5%	
	$\rightarrow HCOH + H_2$		-255 kJ mol^{-1}
	$\rightarrow CH_2$ ($\tilde{a}^1A_1$) + H_2O	1.5 %	-179 kJ mol^{-1}
	$\rightarrow CH_4 + O(^3P_j)$	1.5 %	-190 kJ mol^{-1}

This overview shows not only that there are several competitive channels, but also that production of CH_3 + OH is not the lowest energy channel. This is also illustrated in Fig. 1, which is based on the best experimental data and theoretical calculations presently available.[2,73,85,86,87,88,89] Figure 1 illustrates that

one reason the lower energy products are not favored is the presence of significant potential energy barriers separating the methanol well from these lower energy asymptotes.

Lee and coworkers also studied the atomic and molecular hydrogen channels in crossed molecular beams. They found that the H_2 product was isotropically distributed, suggesting that this channel is likely to be formed in a statistical process. For the atomic hydrogen channel about 90 % of the product was isotropically spread, which again supports an intermediate in which energy is randomized prior to dissociation. However, the remaining 10 % was back scattered, suggesting that an abstraction-like mechanism operates in parallel. They also concluded that the partner species for this channel was more likely to be hydroxymethyl (CH_2OH) rather than the methoxy radical (CH_3O). This finding further provides evidence for a long-lived intermediate, because although the former is ≈36 kJ mol^{-1} lower in energy than the latter, to form CH_2OH the CH_3OH* complex must live long enough for energy to migrate to the CH bond. Doppler spectra of the H atom have consistently measured that about 20 % – 23 % of the available energy appears in translation. Bersohn and coworkers, have also concluded from comparing H atoms for photolysis of methanol and Doppler spectra of nascent H from reaction of $CH_4 + O(^1D_2)$, that an intermediate existed.[18] They estimated that its lifetime was ≈0.8 ps. This lifetime is commensurate with the 0.5 ps that we have assigned to for the dissociation of a CH_4O* intermediate. While it is clear that further studies will be needed to fully elucidate the dynamics of these minor channels, the data support our identification of an intermediate specie following insertion as the principle mechanism.

Evidence suggests that a CH_3OH* intermediate dissociates to form $CH_2OH + H$, $CH_3 + OH$, $H_2CO + H_2$, and CH_2 (ã) + H_2O, which begs the question of whether the quantum yields are consistent with this idea. Our results suggest that 67 % of OH(v=0), 15 % of OH(v=1), and 3 % of OH(v=2) are formed by decay of such an intermediate. These percentages and the measured ratios[6] v = 0/1/2 = 0.25/0.25/0.33 imply that ≈21% of the total OH is formed via the RRKM intermediate. Therefore, ≈14% of the total reactive collisions result in formation of CH_3OH* followed by statistical dissociation to $CH_3 + OH$. According to work mentioned in the preceding paragraph,[20] 23% of the reactive scattering gives $CH_2OH + H$, of which 90% is isotropically scattered, representing decay of a long-lived intermediate. This implies that ≈21% of reactive collisions result in formation of CH_3OH* followed by statistical dissociation to CH_2OH +H. An additional 5% is ascribed to $CH_3OH^* \rightarrow H_2CO + H_2$, and 1.5% to $CH_3OH^* \rightarrow CH_2$ (ã) + H_2O. Is the decay of CH_3OH* into these four channels in the ratio 14/21/5/1.5 reasonable? One expects loose, barrierless transition states for the two simple bond-

breaking channels. The CH_3 + OH channel is favored by a slightly lower energy than CH_2OH +H, and one expects it to be ≈50% faster on that basis. However, the latter channel is triply degenerate, favoring it by a factor of 3. The net expectation for decay of CH_3OH^* is close to the 14/21 ratio deduced from the experiments. The CH_2 (ã) + H_2O channel, although essentially isoenergetic with the OH channel, appears to require an unlikely transition state (low Arrhenius A-factor), resulting in its much lower branching ratio. Presumably this is also the reason for the low yield of H_2, despite its being much lower in energy than the other three channels. Therefore, one may plausibly ascribe the indicated fractions of these four different reactions to statistical decay of a CH_3OH^* intermediate. An implication of this is that the slow OH formation time we determined ($\tau_{slow} \approx 5.4$ ps ± 0.3 ps) is the total decay time of the CH_3OH^* precursor to the four reactive channels. One would predict that if H, CH_2 (ã), or H_2, were probed, the same 5.4 ps formation time would be found. If so, then the identification could be made: k_{uni} = 1/5.4ps = k(OH) + k(H) + k(CH_2 (ã)) + k(H_2), where the ratio of unimolecular rate constants (at ≈50,000 cm^{-1} in the CH_3OH^*) is in the ratio 14/21/5/1.5 deduced above.

Summary of Comparison to Other Results. The above comparison of our time- and state-resolved results to experiments on chemical branching ratios, chemical quenching and chemical kinetics, molecular beam scattering, Doppler profiles, and product states suggests that our simple three mechanism model appears to be consistent with a significant body of research on the title reaction.

Appendix B: Energy Release in OH from the Infrared Multiphoton Dissociation of CH_3OH

In our analysis of the CH_4 + $O(^1D_2)$ → CH_3 + OH reaction, we identified one reaction mechanism as $O(^1D_2)$ insertion followed by the dissociation of vibrationally excited CH_3OH in which vibrational energy was statistically distributed. Therefore, it may prove insightful to examine the results for the distribution of energy in OH formed by dissociation of methanol following laser-induced, infrared multiphoton dissociation (IRMPD). The IRMPD excitation occurs on the 10 ns – 100 ns time scale, guaranteeing that energy is randomized in the molecule before dissociation. Hence, the OH produced from IRMPD of CH_3OH should be truly characteristic of a statistical, unimolecular dissociation.

In this Appendix we present data on OH from the IRMPD of CH_3OH obtained in 1981 but never before published. We analyze this data, along with that published by other groups, and conclude that the dissociation of vibrationally excited CH_3OH leads to OH fragments that are characterized by an unconstrained prior. This conclusion supports our association of the rovibrational distribution

characterized by a zero-slope surprisal with a statistical mechanism for the photolysis-induced $CH_4 \bullet O_3$ cluster reaction. It also supports the conclusion that the mechanisms giving hotter and colder OH are not the dissociation of a methanol molecule in which energy is randomized.

In our IRMPD experiments, neat CH_3OH flowed at a pressure of 0.2 Pa - 0.8 Pa through the photolysis region where CO_2 pump- and ultraviolet probe-lasers propagated collinearly in opposite directions. The CO_2 laser [P(18) line at 1048.7 cm^{-1}] produced temporal "square wave" laser pulses 50 ns duration for our standard measurements.[90,91] Both CD_3OH and CH_3OH were photolyzed, with no significant difference in the rotational state distribution of the OH product. In the OH rotational state measurements, the time delay between the photolysis pulse and the probe pulse was 10 ns. The product yield was linear in probe energy and CH_3OH concentration, and the curve of yield versus time resembled the integral of the cross-correlation between the 50 ns photolysis and 6 ns probe pulses. Figure 12 shows the rotational state distribution of OH(v=0) measured in three different experiments following photolysis of methanol by 75 mJ pulses (fluence F ≈ 38 J cm^{-2} and intensity I ≈ 8×10^8 W cm^{-2}). The data is displayed as a Boltzmann plot. The rotational "temperature", T_R, ≈ 890 K. The state-averaged Λ-doublet ratio was 1.9 ± 0.4, close to the statistical value for high rotational states.

Our results may be compared to two published IRMPD studies. Bialkowski and Guillory[92] first reported LIF measurements of OH rotational states. Their experiments, using a standard CO_2 laser (≈150 J cm^{-2}), were conducted at ≈12 Pa, and hence were not collisionless. An extrapolation suggested a nascent OH(v=0) distribution approximated by T_R = 1250 K ± 400 K. Later, Schmiedl, Meier, and Welge (SMW)[93] used LIF to probe OH(v=0, N=1–7) from CH_3OH in a pulsed molecular beam, presumably under collision free conditions. They measured a distribution approximated by T_R = 630 K ± 60 K after photolysis with a multimode CO_2 laser, for which the fluence and intensity were considered not well defined (F ≈ 100 J cm^{-2}). The ratio of spin-orbit states was found to be ≈1.3. This is similar to the value of 1.3 reported by this laboratory for OH from $CH_4 \bullet O_3$ and by Wada and Obi for OH (v=0, N=3–7) formed in photolysis of the $CH_4 \bullet N_2O$ complex. This is slightly higher than the ratio of 1.0 found by Luntz,[60] Park and Wiesenfeld,[6] and Wada and Obi[27] for the free, bimolecular $CH_4 + O(^1D_2)$ reaction. SMW used Doppler spectroscopy to estimate the translational energy of the OH(v=0) products. Their fits to the Doppler profile gave widths in the range 3.96 GHz – 2.83 GHz, depending of the fitting procedure The fit corresponding to 3.96 GHz drawn in their Fig. 3 is actually broader than the data. For $\Delta\upsilon$=3.96 GHz, the deconvolution of the 1.4 GHz laser bandwidth gives a 3.7 GHz Doppler width. If instead one takes the average of the two fits shown in SMW Fig. 3, then one

would deduce a Doppler width of 3.2 GHz. Assuming an isotropic, Gaussian speed distribution, $\Delta\upsilon$=3.7 GHz implies a translational temperature, T_t, of ≈400 K, and $\Delta\upsilon$=3.2 GHz implies $T_t \approx 300$ K. The translation energy in the fragment is $E_{trans,OH} = \frac{3}{2}kT_t$ and $E_{trans,CH_3} = \frac{m_{OH}}{m_{CH_3}} E_{trans,OH}$,where k represents Boltzmann's constant and m_{OH/CH_3} represents the mass of the hydroxyl and methyl radicals, respectively. If one takes T_t = 400 K, then the average translational energy release is 890 cm^{-1}, while T_t = 300 K gives 670 cm^{-1}.

These IRMPD data can be compared to prior distributions calculated as discussed above. A prior distribution for an available energy of 2000 cm^{-1} corresponds to an OH(v=0,J) distribution well approximated by a rotational temperature of $T_R \approx 630$ K, and an average translational energy release of ≈690 cm^{-1}. These are consistent with the experimental IRMPD results of SMW. Shown overlaid on our data in Fig. 12 is the calculated prior distribution for a CH_3OH^* energy of 3000 cm^{-1}, which is in good agreement with the data. Even better agreement could be obtained by assuming that some CH_3OH molecules absorbed (n) 1049 cm^{-1} photons and some absorbed (n+1) photons, where n ≈ 34, so that the average of priors for 2475 cm^{-1} and 3525 cm^{-1} above threshold is used. Therefore, if the dissociating CH_3OH actually had the amount of vibrational energy assumed in the prior calculations, then the IRMPD data show that CH_3OH, with statistically distributed vibrational energy, gives a statistically distributed OH product. Evidence that this is correct comes from RRKM calculations of the CH_3OH^* dissociation rate, *k(E)*, as a function of energy, *E*.

We calculated RRKM dissociation rates, consistent with the experimental high pressure Arrhenius A-factor of $A_\infty = 10^{16}$ s^{-1}, using a standard computer program[94] and sensible transition state parameters.[95] This transition state gave a dissociation rate at 16,600 cm^{-1} was 2.0×10^{11} s^{-1}, consistent with the τ_{slow} = 5 ps observed for the slowest OH formation rate in the $CH_4 \bullet O_3$ cluster experiment. At lower energies relevant to the IRMPD experiments, 1 to 4 photons above threshold, the same calculation gave *k(E)* = 0.21, 0.94, 2.9, and 7.3×10^8 s^{-1} (dissociation times of 47 ns, 11 ns, 3.4 ns, and 1.4 ns). That is, at an energy ≈2 photons above threshold, *k(E)* increases by about a factor of four as E increases by ≈1000 cm^{-1} . In the next paragraphs, this *k(E)* calculation that fit the CH_3OH^* lifetime measured in the cluster experiment is also seen to fit the IRMPD data.

A standard model of IRMPD experiments is that the reactant absorbs laser photons until it reaches a level of vibrational excitation above threshold where the rate of further up-pumping is balanced by the rate of unimolecular dissociation.[96] One expects dissociation rates to increase rather

rapidly with increasing energy above threshold. One does not expect the absorption cross section, σ, to vary rapidly with vibrational excitation for the level of excitation involved in the reaction $CH_3OH \rightarrow CH_3 + OH$ (≈34 photons). One expects the CH_3OH to be pumped to a higher vibrational level for which the dissociation rate increases linearly in the laser intensity, *I*,

$$k(E) = \sigma I \qquad \text{(B1)}$$

where E is the average energy of the molecules that dissociate.[91] Therefore, higher intensity excites CH_3OH^* to levels for which *k(E)* is greater, i.e., *E* is greater, giving products with more energy than from a lower intensity pump. We measured the distribution OH(v=0, J, Ω, Λ) for pump laser pulses of different intensities. At constant fluence (≈38 J cm^{-2}) we compared 50 ns, "square-wave" pulses ($\approx 8 \times 10^8$ W cm^{-2}) to longer non-modelocked, 200 ns FHWM Gaussian pulses ($\approx 2 \times 10^8$ W cm^{-2}). With this decrease in peak intensity by four, Eq. (B1) suggests E decreases such that *k(E)* should decrease by about four. In the experiment, the OH product decreased in energy from a distribution fit by $T_R \approx 890$ K to one fit by $T_R \approx 680$ K. This change in OH rotational energy is consistent with the prior expectation for CH_3OH^* dissociating from $E \approx 3000$ cm^{-1} above threshold compared to $E \approx 2000$ cm^{-1}. The RRKM calculation showed that *k(E)* should decrease by a factor of four in this energy range. Therefore the observed scaling of OH product energy with laser intensity is that expected for CH_3OH^* dissociating statistically.

The question arises whether these calculated dissociation rates are observed in the IRMPD experiments and whether the steady-state condition necessary for Eq. (B1) to be applicable was realized for the results presented here. Several observations can answer these questions. First, in the IRMPD experiments using the square-wave laser pulse, OH production ended when the pump laser switched off, to within the 10 ns time resolution of the experiment. This suggests reaction from CH_3OH^* levels with lifetimes <10 ns, as predicted by the RRKM calculation. Second, dissociation using 50 ns laser pulses (≈38 J cm^{-2}; $\approx 8 \times 10^8$ W cm^{-2}) gave OH with $T_R \approx 890$ K. In contrast, dissociation by a laser of shorter duration (2 ns) but higher intensity (≈7.6 J cm^{-2}, $\approx 3 \times 10^9$ W cm^{-2}) gave OH with $T_R \approx 620$ K. This observation shows that the more intense 2 ns pulses do not last long enough for the steady-state condition to be realized, inasmuch as if steady-state had been achieved the products would have been hotter than those produced by pulses of lower peak intensity. This suggests that the CH_3OH dissociates from states with lifetimes not much shorter than 2 ns, as calculated in the paragraph above. Third. the IRMPD experiments were modeled using rate equations for the stimulated up- and down-pumping of the CH_3OH and unimolecular reaction rates given by RRKM calculations. These calculations confirm

that with reasonable choices for the laser pumping rate σI (*e.g.*, $\sigma \approx$ v+1, or $\sigma \approx$ constant), the essential experimental results may be reproduced, including: absorption of 32-35 photons, dissociation from levels in the region 2-4 photons above threshold, the observed OH formation timescale, and the observed dependence of the rotational temperature on the laser duration and intensity. These observations are consistent with the hypothesis that in the IRMPD experiments reported here, the dissociation occurs on a timescale and give a product state distribution that are predicted by statistical theory.

It is quite possible for an IRMPD dissociation to give extremely non-statistical product energy distributions, despite statistical distribution of energy in the reactant. Such cases usually involve a tight, or constrained transition state,[96] or are the manifestation of selection rules for a curve crossing, and have large barriers to the reverse reaction.[97] The dissociation of methanol is spin-allowed and it involves a loose transition state, as evidenced by the high Arrhenius A-factor. There is no barrier to the reverse reaction, as the small and statistical translational energy release in the IRMPD dissociation proves. This conclusion about lack of barriers to reaction was also reached in kinetic studies[22] that found a CH_3 + OH recombination rate at room temperature of 7×10^{-11} cm^{-3} s^{-1}, a rate for OH + $CH_3 \rightarrow CH_2(\tilde{a})$ + H_2O of 3×10^{-11} cm^{-3} s^{-1}, and a rate for $CH_2(\tilde{a})$ + $H_2O \rightarrow CH_3$ + OH of 1.5×10^{-10} cm^{-3} s^{-1}, rates all close to gas kinetic. Therefore, the dissociation of CH_3OH^* is a case with few dynamical constraints to cause surprising product energy disposal. The IRMPD results give strong support to the idea that the CH_3OH dissociation is statistical.

Figure Captions

Figure 1 – A correlation diagram for the reaction between methane and atomic oxygen. The heats of formation and barrier heights are based on Refs. 2, 73, 85-89.

Figure 2 – The circles are the OH LIF signal from the photolysis of H_2O_2. The line is the pump/probe integrated cross correlation shifted by 25 fs. The squares are the OH LIF signal for the CH_4•O_3 cluster probed at 316.5 nm. The data are normalized so that the fast component in the cluster photolysis and the H_2O_2 signal have the same height at long time.

Figure 3 – Shown here is a portion of the LIF spectrum of OH formed following photolysis of the CH_4•O_3 cluster. Superimposed on the state-resolved spectrum is the power spectrum of the probe laser at 308.8 nm.

Figure 4 – The OH(v=0,1) population distributions for each Λ-doublet and spin-orbit state. The intensities for v=0 and 1 are on the same scale.

Figure 5 – The dots show the measured OH LIF data for the CH_4•O_3 cluster reaction as a function of pump/probe delay time. The asymptotic value for each data set is unity. The lines represent the optimization of Eq. (9) to the experimental points. The wavelength probed is shown below each line.

Figure 6 – The dots show the measured OH LIF data for the CH_4•O_3 cluster reaction as a function of pump/probe delay time for short time delays. The asymptotic value is set to unity. The dashed lines represent the optimization of Eq. (3), the two-mechanism fit, and the dots close to the top of the panels are the residuals. The solid lines represent the optimization of Eq. (9), the three-mechanism fit, to the experimental points and the residuals are shown below the other residuals. The wavelength probed is shown below each set of data.

Figure 7 – The circles are the C_i^f determined from the time-resolved data for each data set. The squares are the C_i^f calculated from Eq. (5) based on the Boltzmann optimization to the state resolved data, Eq. (6). The diamonds are the C_i^f calculated from Eq. (5) based on the surprisal optimization to the state resolved data, Eq. (8). This shows that neither the approach of Eq. (6) or (8) gives coefficients close to those that fit the time-resolved data.

Figure 8 – The symbols show the OH(v=0,1) rotational population data displayed as a Boltzmann plot. The lines give the two temperature Boltzmann fit via Eq. (5).

Figure 9 – Surprisal plots for OH(v=0,1) showing surprisal as a function of reduced rotational energy. The dashed lines are the optimizations of Eq. (8), the two-mechanism model, to the OH surprisals for v = 0 and v = 1. The solid lines are the optimization of Eq. (10), the three-mechanism model.

Figure 10 – Displayed is a comparison between the $C_i^{f\,/i/s}$ determined from the time-resolved data and the $C_i^{f\,/i/s}$ calculated from the surprisal fits. The open symbols are from the time-resolved data and the

filled symbols are calculated from the surprisal fits. The squares are the C_i^f 's for the cold distribution and fast time constant. The circles are the C_i^i 's for the hot distribution and intermediate time constant. The triangles are the C_i^s 's for the statistical distribution and slow time constant.

Figure 11 – Fraction of the OH(v=0,1) rotational state populations calculated for the three mechanisms: abstraction (squares), insertion/elimination before complete IVR (circles), and statistical dissociation of a long-lived methanol intermediate (triangles).

Figure 12 – Rotational distribution for OH(v=0, N, f_1) from IRMPD of CH_3OH, displayed as a Boltzmann plot. Open circles show the data and closed triangles the prior distribution calculated for internal energy 3000 cm^{-1} above threshold.

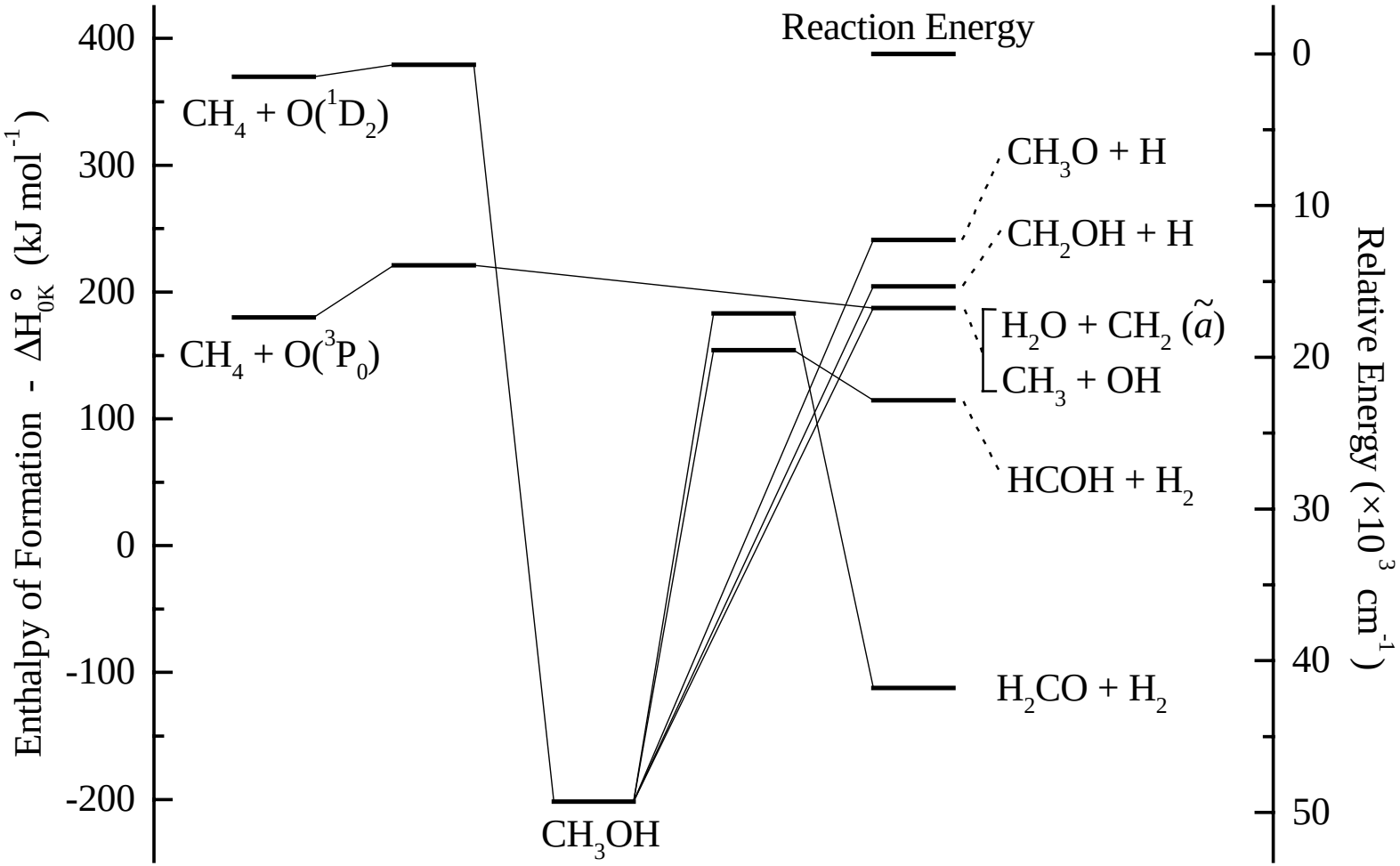

Miller, van Zee and Stephenson Figure 1

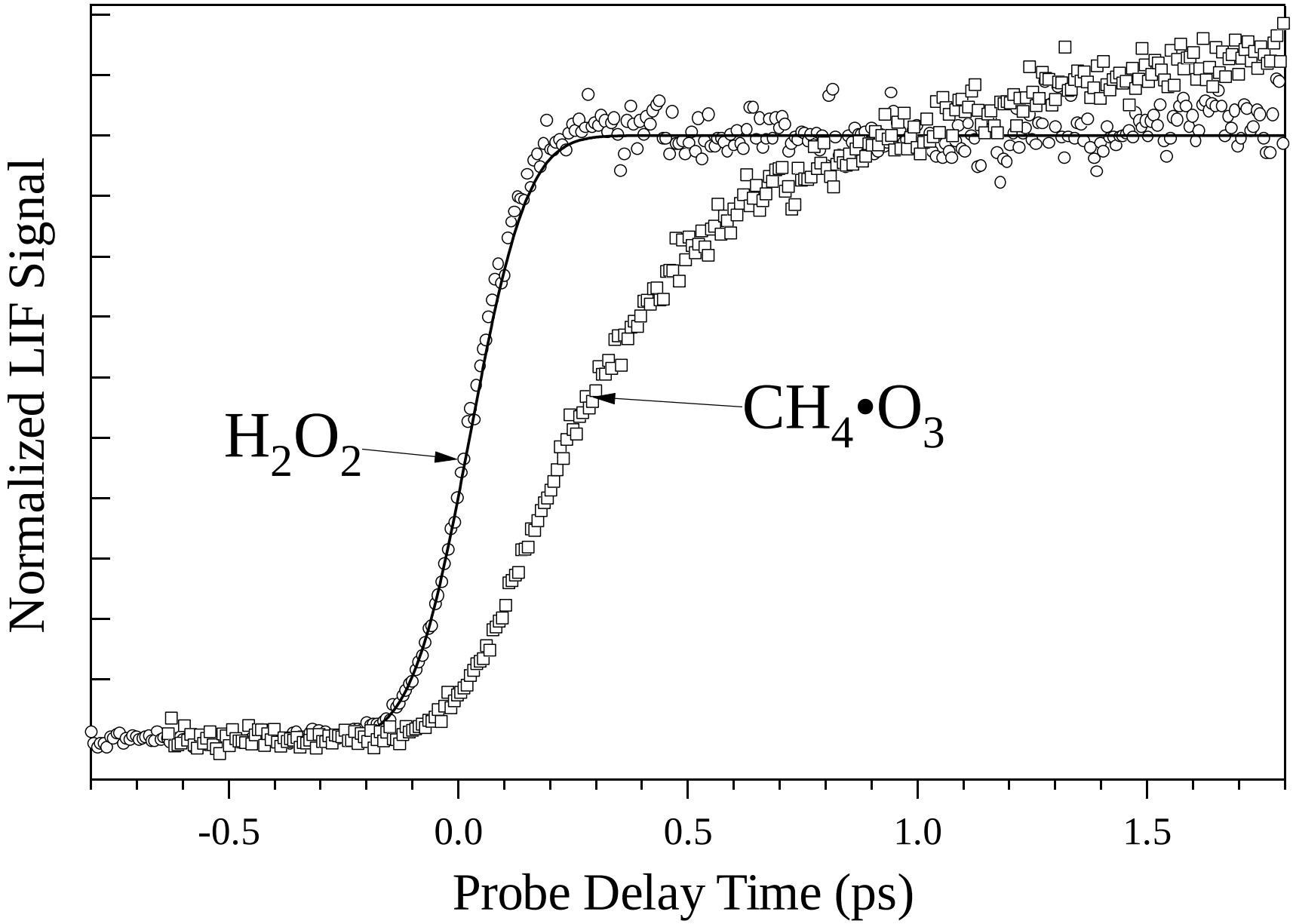

Miller, van Zee & Stephenson Figure 2

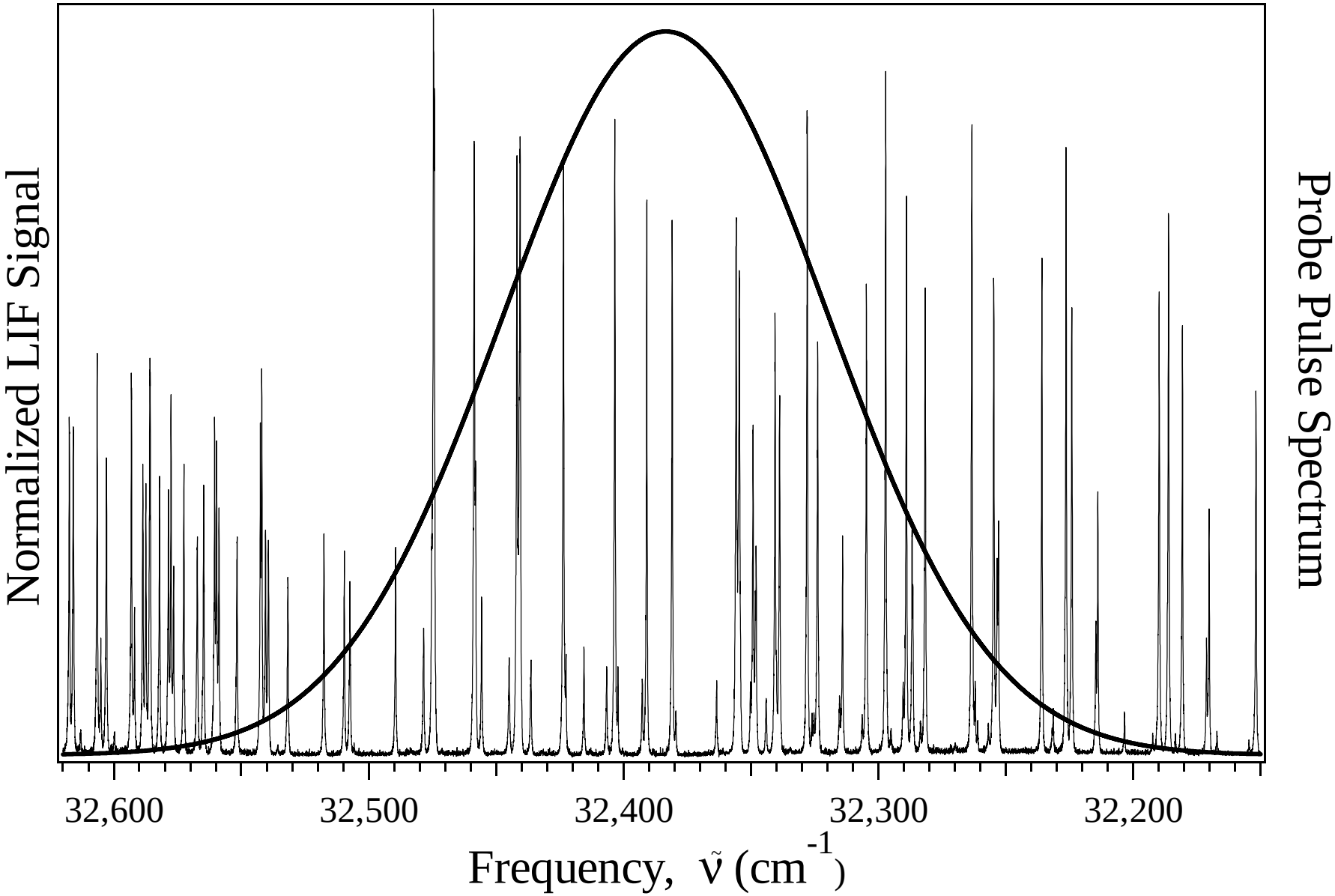

Miller, van Zee & Stephenson Figure 3

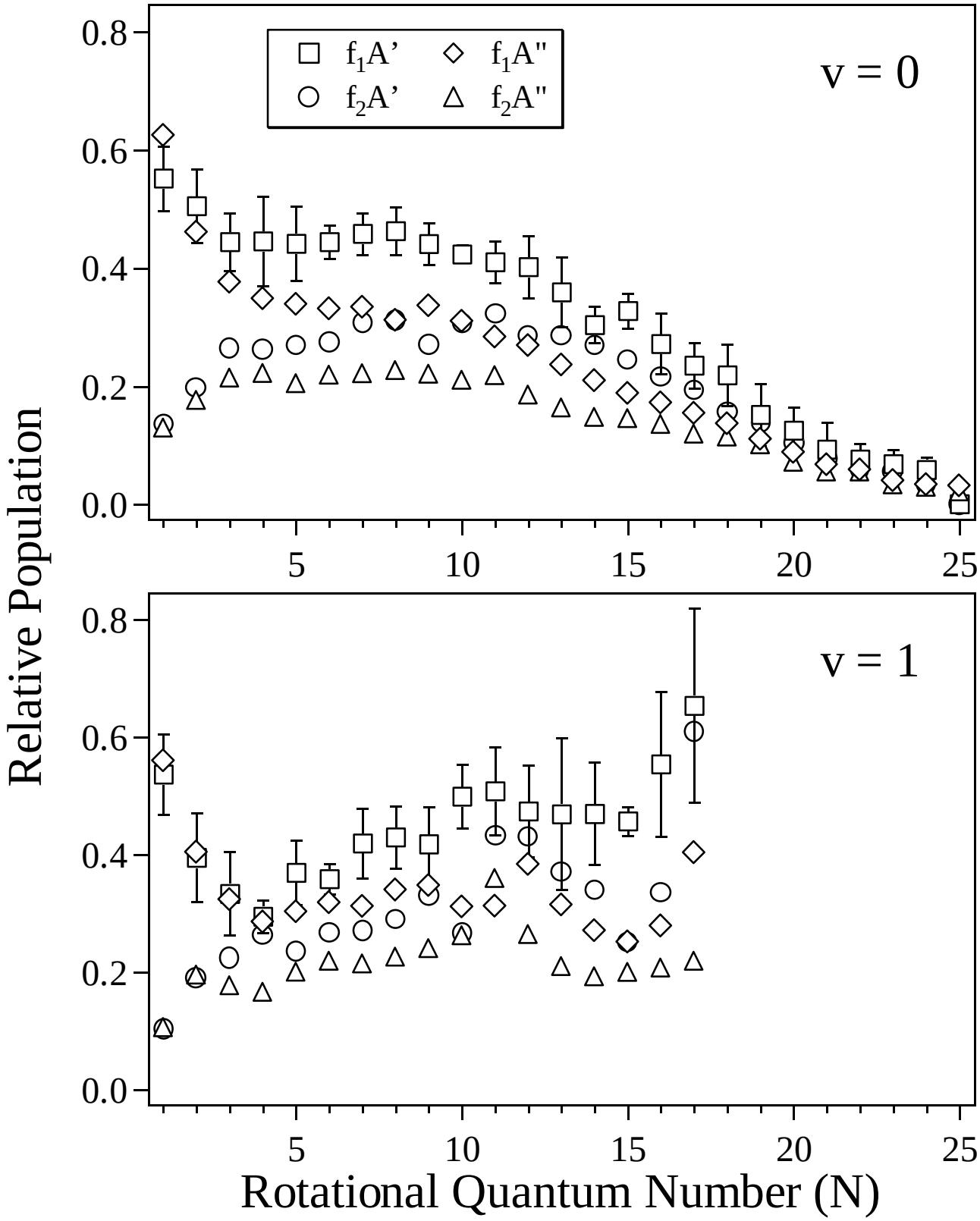

Miller, van Zee & Stephenson Figure 4

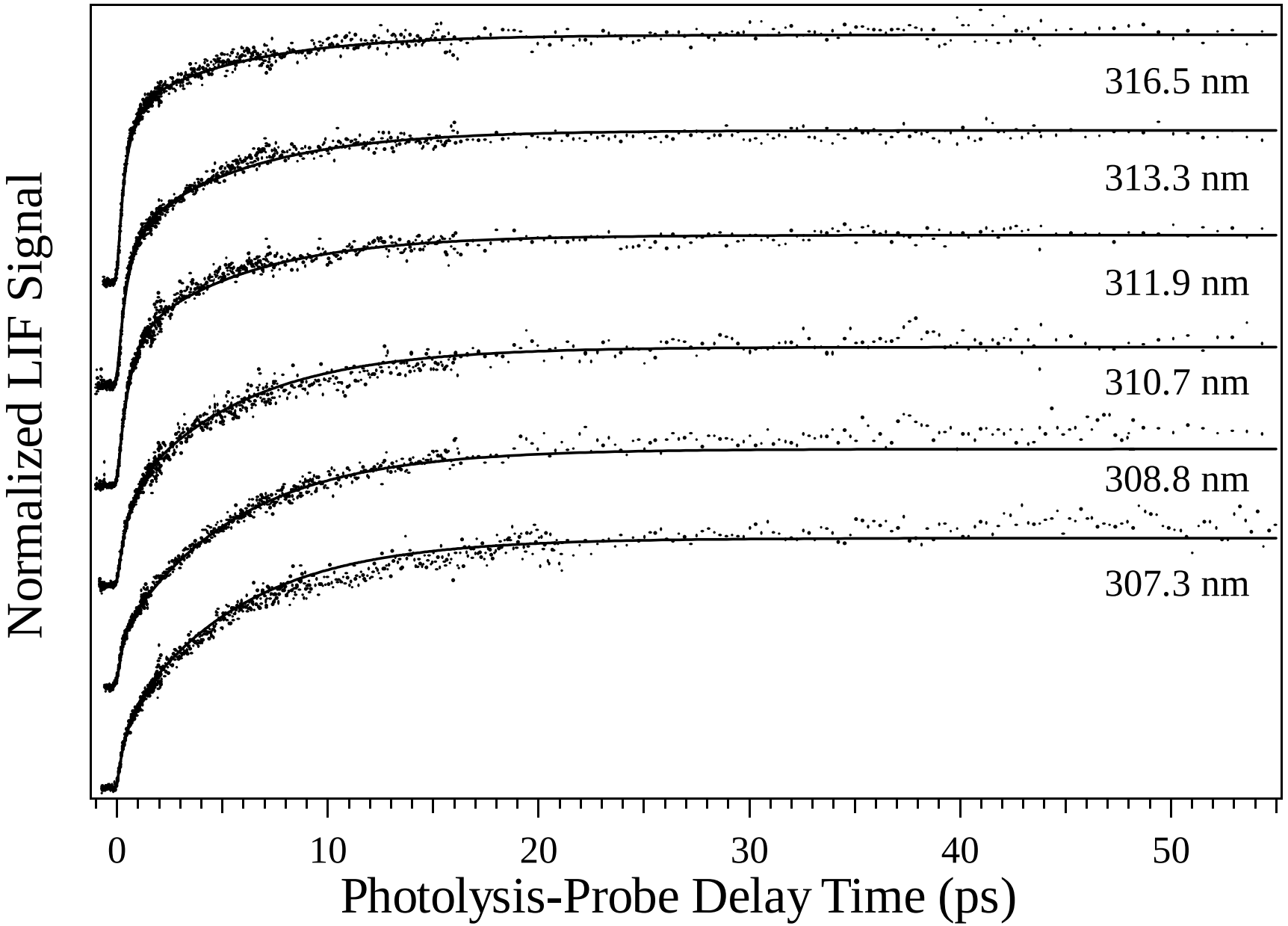

Miller, van Zee & Stephenson Figure 5

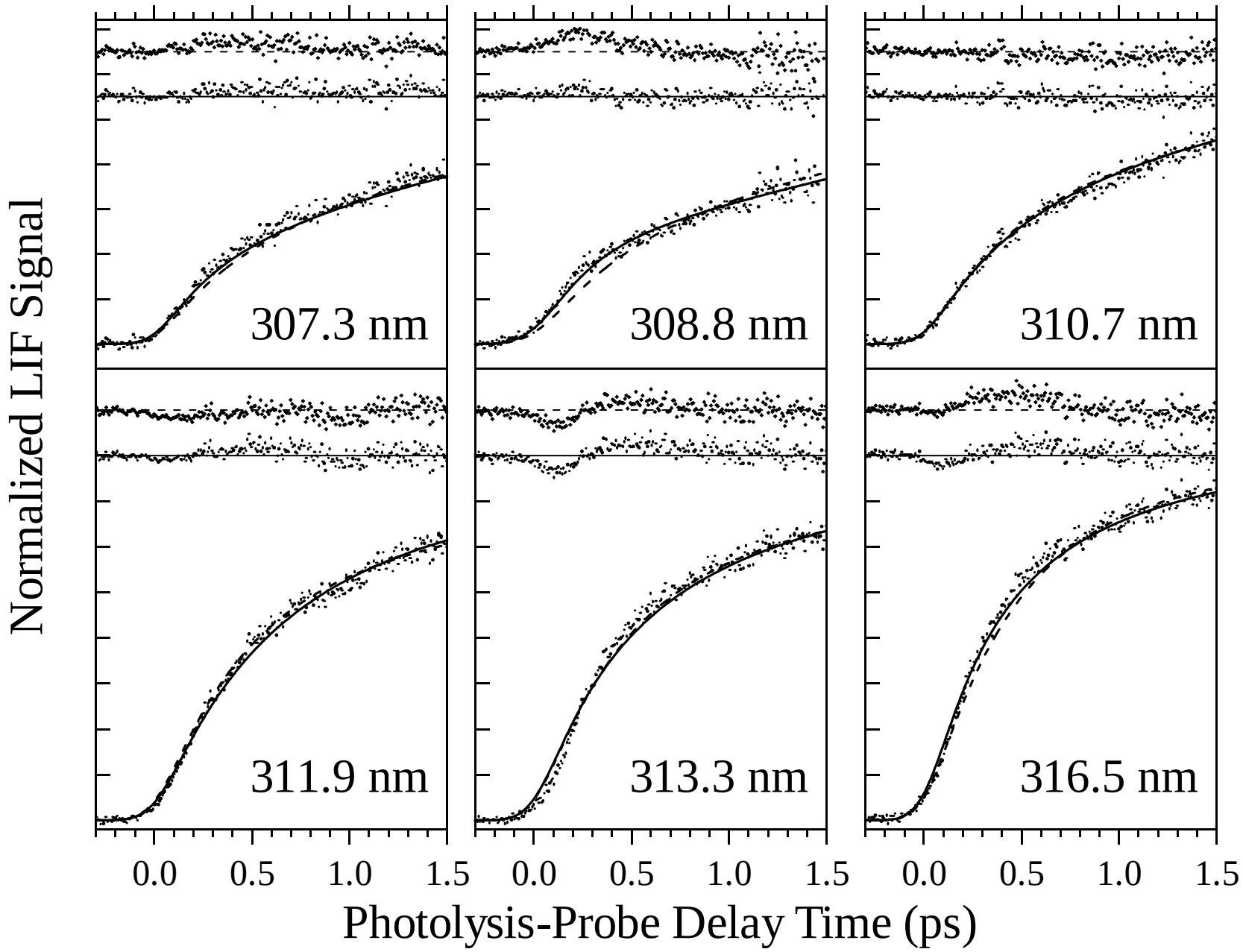

Miller, van Zee & Stephenson Figure 6

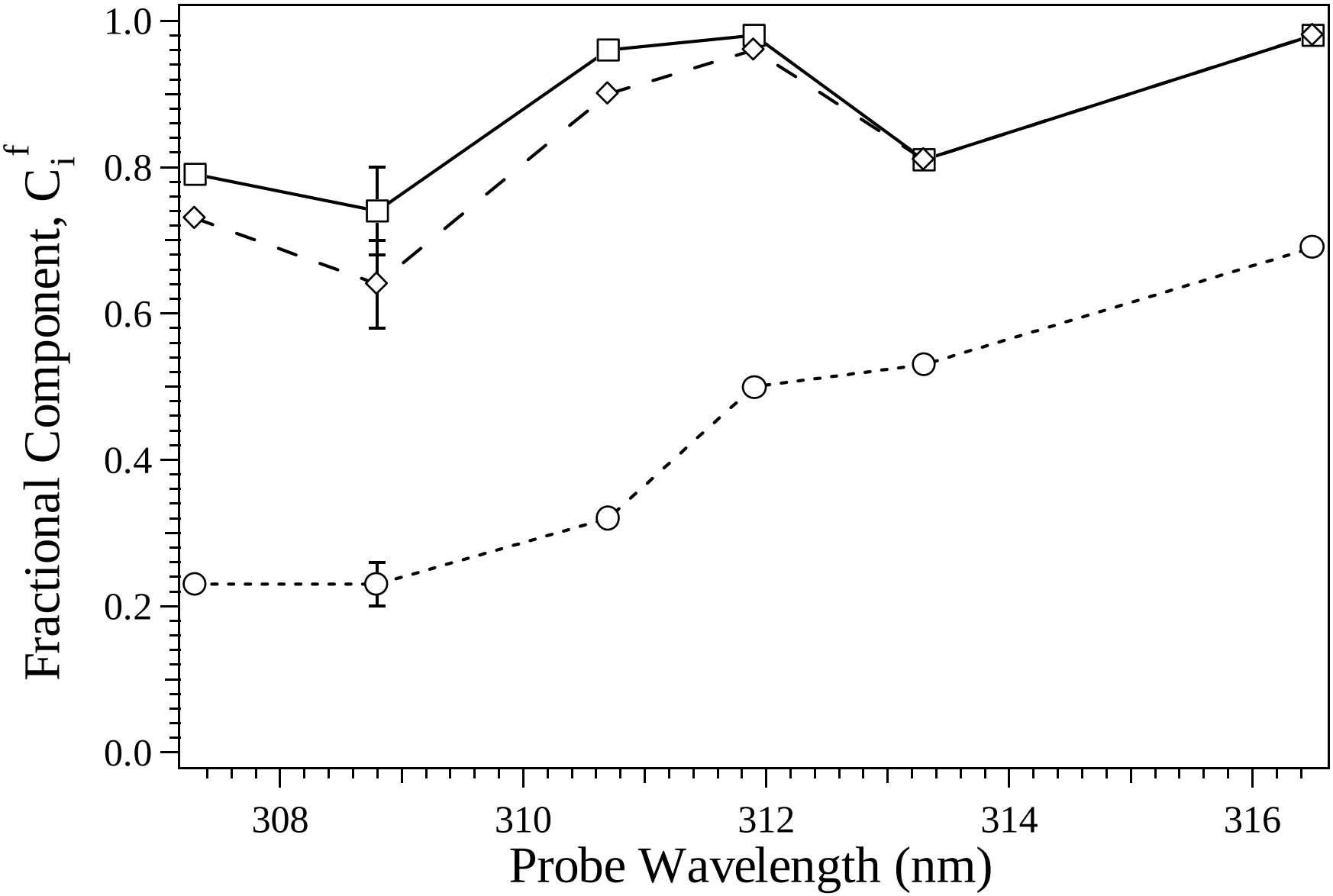

Miller, van Zee & Stephenson Figure 7

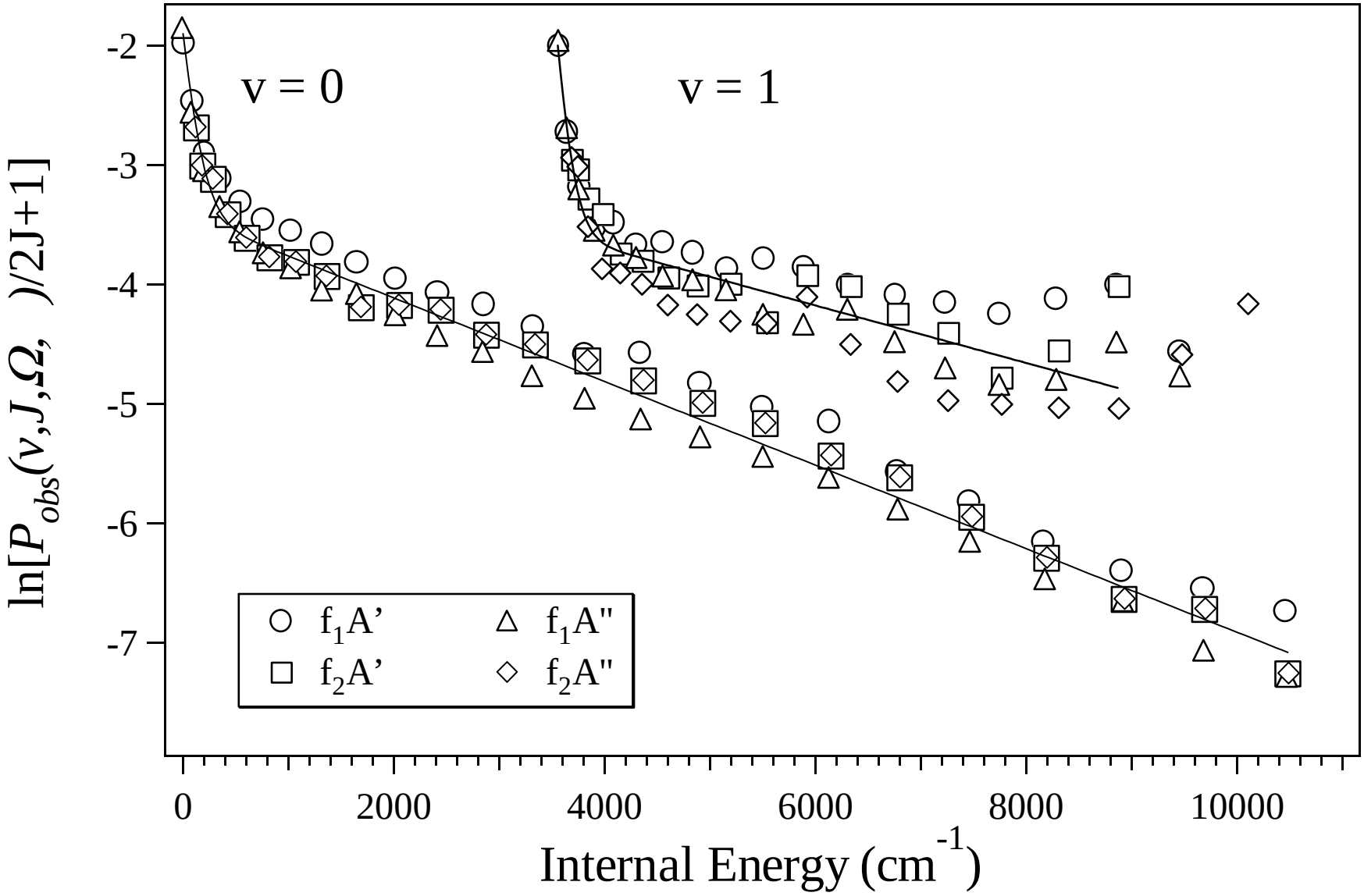

Miller, van Zee & Stephenson Figure 8

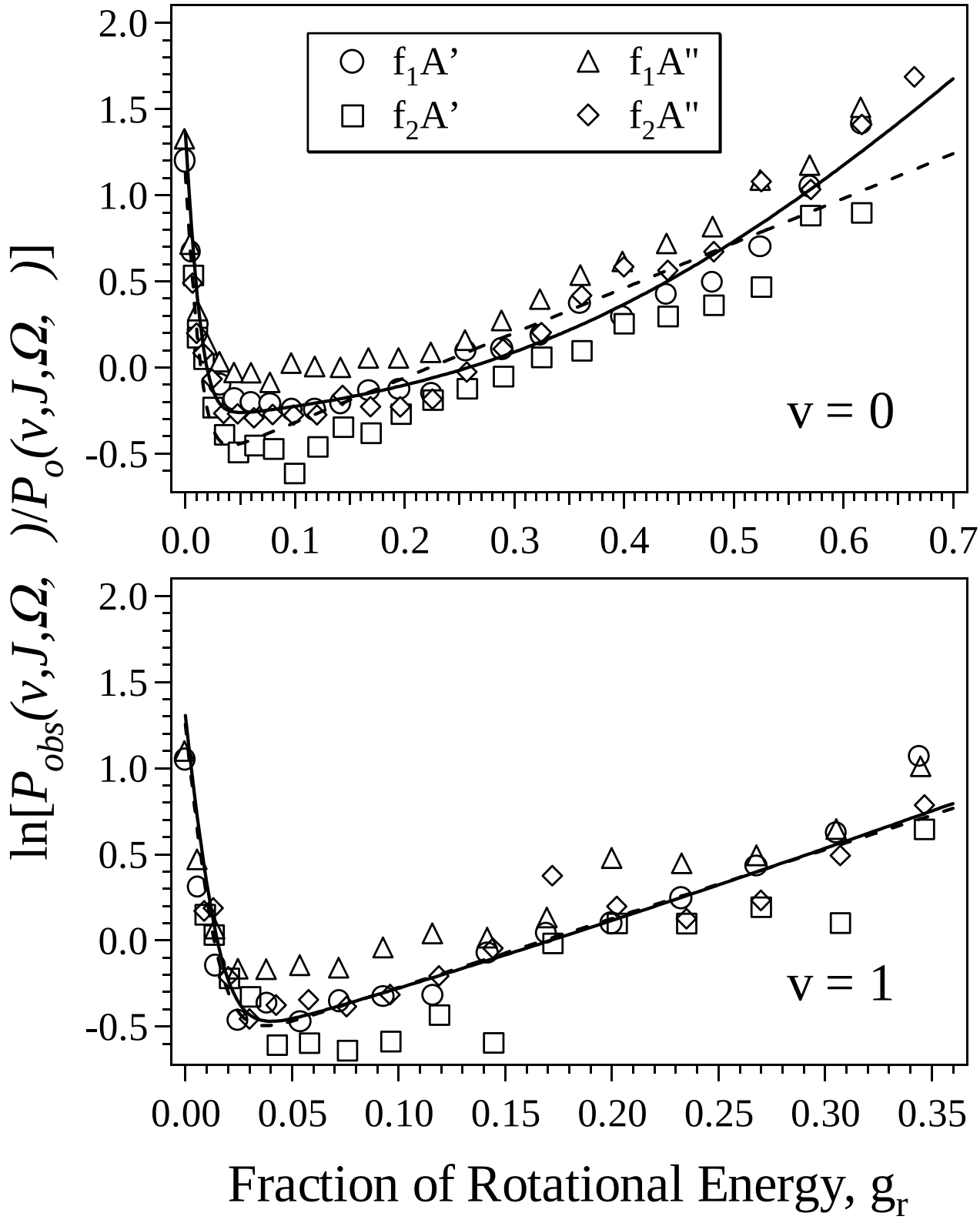

Miller, van Zee & Stephenson Figure 9

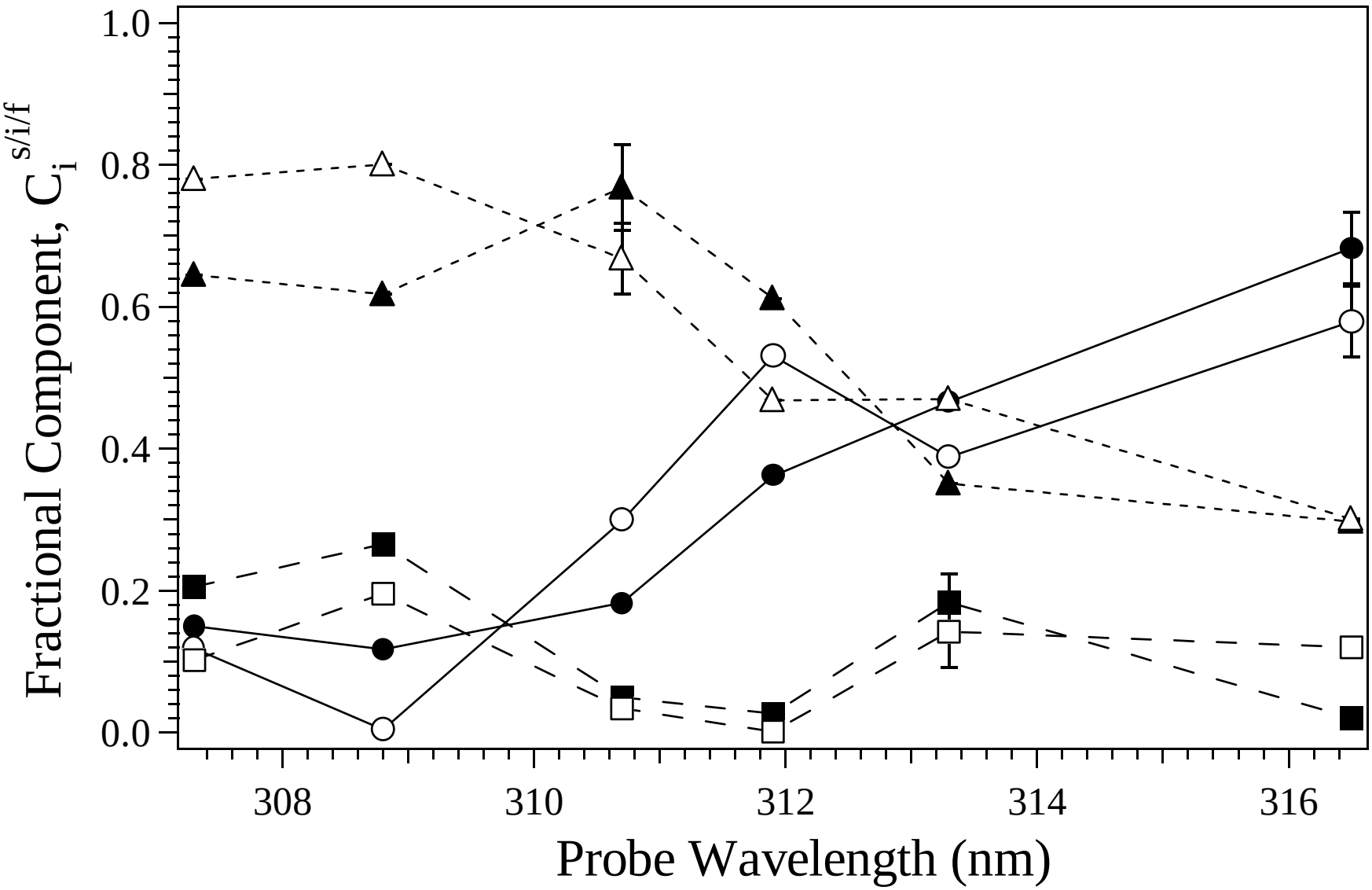

Miller, van Zee & Stephenson Figure 10

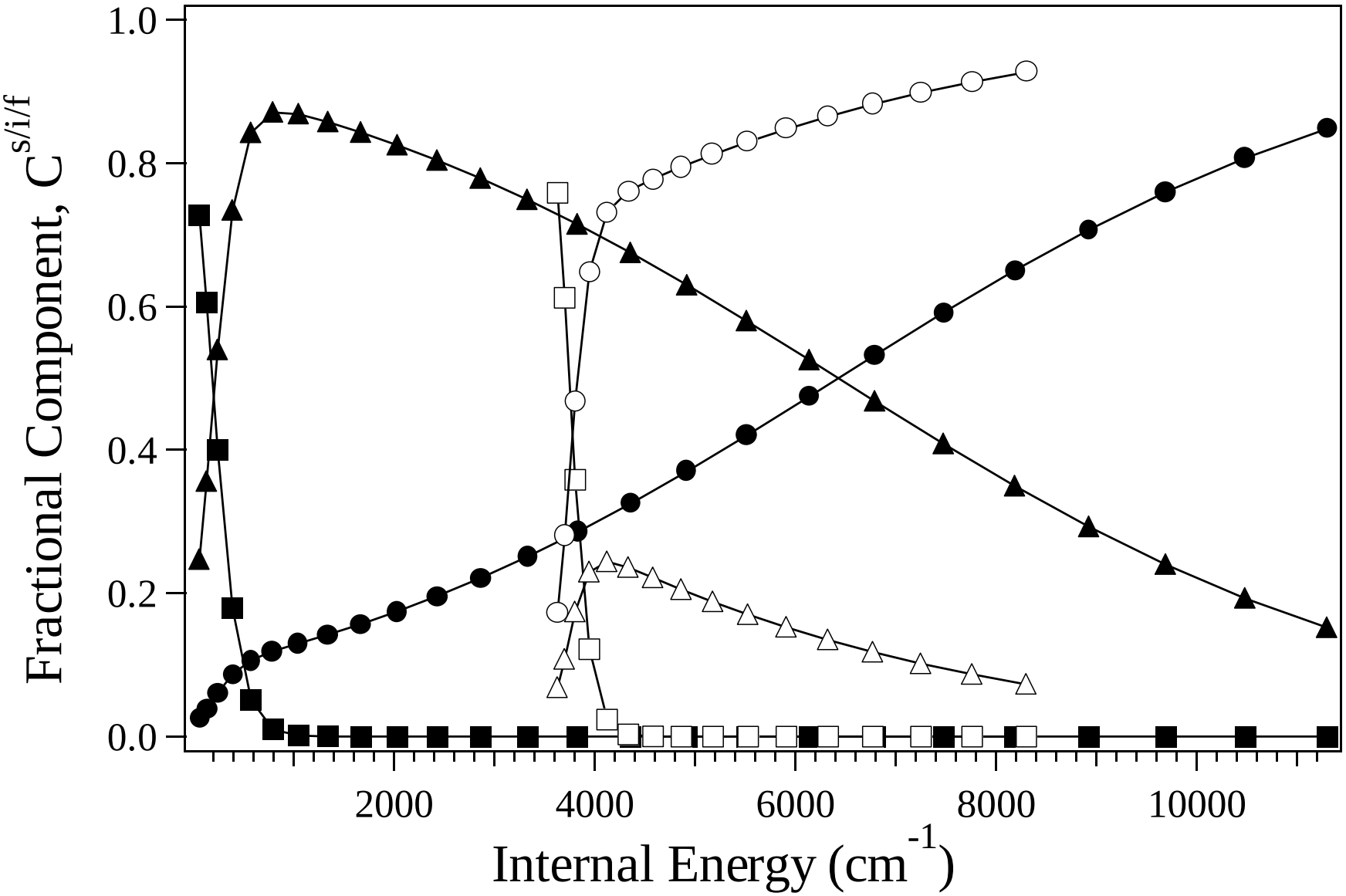

Miller, van Zee & Stephenson Figure 11

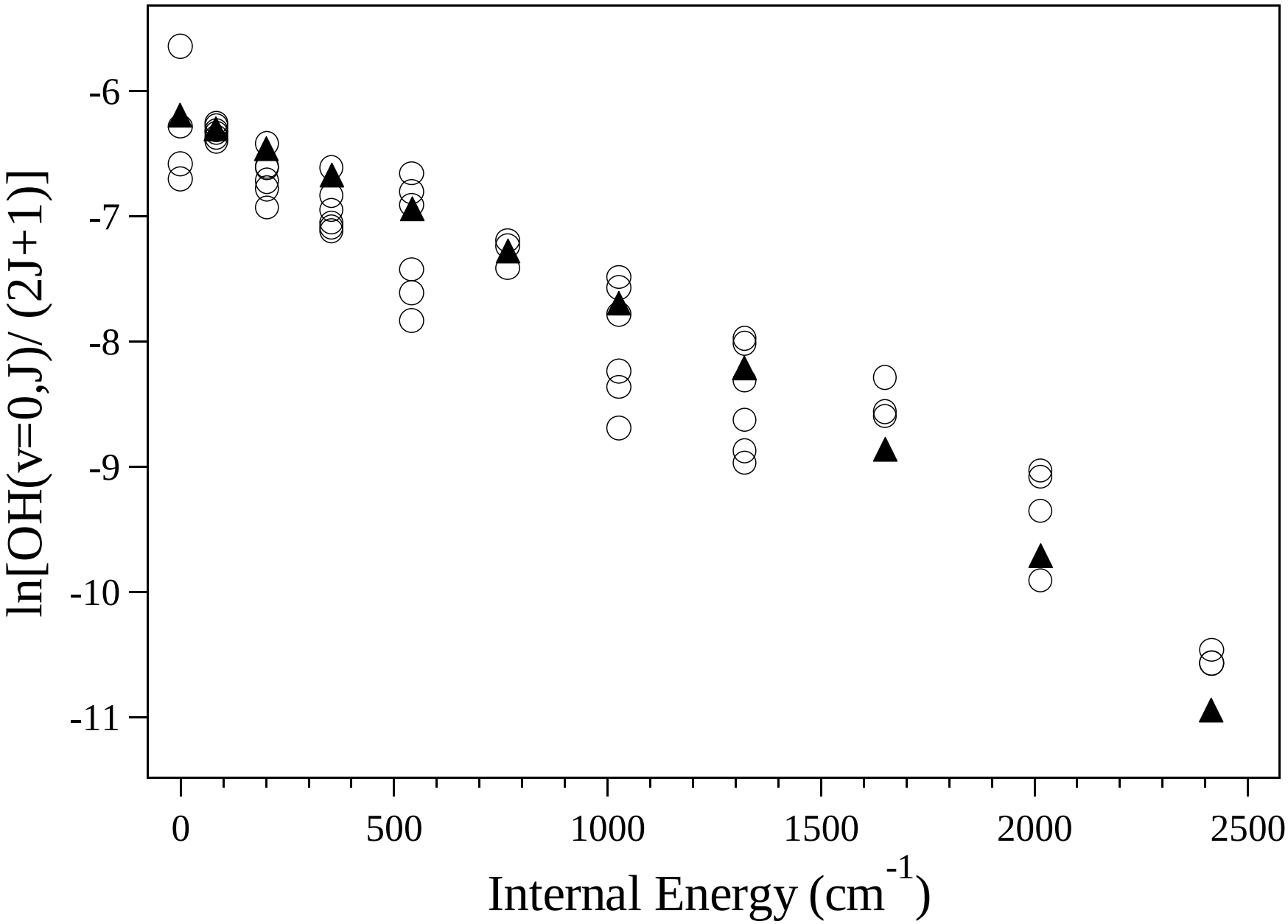

Miller, van Zee & Stephenson Figure 12

References

[1] N. Basco and R.G.W. Norrish, Proc. Roy. Soc. Ser. A, **260,** 293, (1961).
[2] NIST-JANAF Thermochemical Tables, Fourth Edition, Malcolm W. Chase, Jr., Ed. (ACS/AIP, 1998).
[3] C.-L. Lin and W.B. DeMore, J. Phys. Chem., **77**, 863 (1973).
[4] W.B. DeMore and O.F. Raper, J. Chem. Phys., **46**, 2500 (1967).
[5] W.B. DeMore, J. Phys. Chem., **73**, 391 (1969).
[6] C.R. Park and J.R. Wiesenfeld, J. Chem. Phys., **95**, 8166 (1991).
[7] M. Brouard, H.M. Lambert, C.L., Russell, J. Short and J.P. Simons, J. Chem. Soc. Faraday Trans., **102**, 1 (1995).
[8] M. Brouard, H.M. Lambert, J. Short and J.P. Simons, J. Phys. Chem., **99**, 13571 (1995).
[9] M. Brouard, S.P. Duxon and J.P. Simons, Israel J. of Chem., **34**, 67 (1993).
[10] J.P. Simons, J. Chem. Soc. Faraday Trans., **93**, 4095 (1997).
[11] M. Brouard, S.P. Duxon, P.A. Enriquez and J.P. Simons, J. Chem. Soc. Faraday Trans., **89**, 1435 (1993).
[12] T. Suzuki and E. Hirota, J. Chem. Phys., **98**, 2387 (1992).
[13] R. Schott, J. Schlutter, M. Olzmann and K. Kleinermanns, J. Chem. Phys., **102**, 8371 (1995).
[14] J. Schlutter, R. Schott and K. Kleinermanns, Chem. Phys. Letters, **213**, 262 (1993).
[15] H. Arai, S. Kato and S. Koda, J. Phys. Chem., **98**, 12 (1993).
[16] R.A. Brownsword, M. Hillenkamp, P. Schmiechen and H.-R. Volpp, J. Phys. Chem., **102**, 4438 (1998).
[17] Y. Matsumi, K. Tonokura, Y. Inagaki and M. Kawasaki, J. Phys. Chem., **97**, 6816 (1993).
[18] S. Satyapal, J. Park, R. Bersohn and B. Katz, J. Chem. Phys., **91,** 6873 (1989).
[19] J.J. Lin, Y.T. Lee and X. Yang, J. Chem. Phys., **109**, 2975 (1998).
[20] J.J. Lin, S. Harich, Y.T. Lee and X. Yang, J. Chem. Phys., **110**, 10821 (1999).
[21] W. Hack and H. Thiesemann, J. Phys. Chem., **48**, 17364 (1995).
[22] W. Hack, H. Gg. Wagner and A. Wilms, Ber. Bunsenges Phys. Chem., **92**, 620 (1988).
[23] R.D. van Zee and J.C. Stephenson, J. Chem. Phys., **102**, 6946 (1995).
[24] C. Jacques, L. Valachovic, S. Ionov, Y. Wen, J. Segal and C. Wittig, J. Chem. Soc. Faraday Trans., **89**, 1419 (1993).
[25] N.F. Scherer, L.R. Khundkar, R.B. Bernstein and A.H. Zewail, J. Chem. Phys., **87**, 1451 (1987).
[26] I. R. Sims, M. Gruebele, E. D. Potter and A. H. Zewail, J. Chem. Phys., **97**. 4127 (1992).
[27] S.-I. Wada and K. Obi, J. Phys. Chem., **102**, 3481 (1997).
[28] R.D. van Zee, J.C. Stephenson and M.P. Casassa, Chem. Phys. Letters, **223**, 167 (1994).
[29] S. I. Ionov, G. A. Brucker, C. Jacques, L. Valachovic and C. Wittig, J. Chem. Phys., **99**, 6553 (1993).
[30] K. Kühl and R. Schincke, Chem. Phys. Lett., **158**, 81 (1989).
[31] R. Bersohn and M. Shapiro, J. Chem. Phys., **85**, 1396 (1986).
[32] Z.T. Cai, D.H. Zhang and J.Z.H. Zhang, J. Chem. Phys., **100**, 5631 (1994).
[33] R. Bersohn and A.H. Zewail, Ber. Bunsenges. Phys. Chem., **92**, 373 (1988).
[34] G. H. Dieke and H. M. Crosswhite, J. Quant. Spectry. Radiative Transfer, **2**, 97 (1962).
[35] J. Brzozowski, P. Erman and M. Lyyra, Physica Scripta, **17**, 507 (1987).
[36] I. L. Chidsey and D. R. Crosley, J. Quant. Spectry. Radiative Transfer, **23**, 187 (1980).
[37] R. N. Zare, Angular Momentum (Wiley, New York, 1988) p 297 ff.
[38] J. T. Hougen, The Calculation of Rotational Energy Levels and Rotational Line Intensities in Diatomic Molecules, NBS Monograph 115, (U.S. Gov't. Printing Office, Washington DC, 1970).

[39] A. Schiffman, D.D. Nelson and D.J. Nesbitt, J. Chem. Phys., **98**, 6935 (1993).
[40] C.L. Lin, N.K. Rohatgi and W.B. DeMore, Geophys. Res. Lett., **5**, 113 (1978).
[41] M.P. Docker, A. Hodgson and J. P. Simons, Faraday Discuss. Chem. Soc., **82**, 1 (1986).
[42] R.N. Dixon, J. Nightingale, C.M. Western and X. Yang, Chem. Phys. Letters, **151**, 328 (1988).
[43] M.P. Docker, A. Hodgson and J. P. Simons, Chem. Phys. Letters, **128**, 264 (1986).
[44] K.-H. Gericke, A.U. Grunewald, S. Klee and F.J. Comes, J. Chem. Phys., **88**, 6255 (1988).
[45] S. Klee, K.-H. Gericke and F.J. Comes, J. Chem. Phys., **85**, 40 (1986).
[46] K.-H. Gericke, S. Klee, F.J. Comes and R.N. Dixon, J. Chem. Phys., **85**, 4463 (1986).
[47] D.E. Freeman, K. Yoshino, J.R. Esmund and W.H. Parkinson, Planet Space Sci., **32**, 239 (1984).
[48] M.P. Casassa, J.C. Stephenson and D.S. King, J. Chem. Phys., **89**, 1966 (1988).
[49] T. Baer and W.L. Hase, Unimolecular Reaction Dynamics (Oxford Univ. Press, New York, 1996) p.328 ff.
[50] R.B. Bernstein and R.D. Levine, Adv. Atomic Mol. Phys. **11,** 215 (1975).
[51] W. Forst, Chem. Rev., **71**, 354 (1971).
[52] V. Spirko and P.R. Bunker, J. Mol. Spectrosc., **95**, 381 (1982).
[53] T. Baer and W.L. Hase, op. cit., p. 324 ff.
[54] J.L. Kinsey, J. Chem. Phys., **54**, 1206 (1971).
[55] T. Baer and W.L. Hase, op. cit., p. 325 ff.
[56] T. Baer and W.L. Hase, op. cit., p. 188 ff.
[57] M. Olzmann, Ber. Bunsenges Phys. Chem., **101**, 533 (1997).
[58] O.V. Boyarkin, T.R.Rizzo and D.S. Perry, J. Chem. Phys. **110**, 11346 (1999).
[59] R.I. Greenberg and J. Heicklen, Int'l. J. of Chem. Kinetics, **4**, 417 (1972).
[60] A.C. Luntz, J. Chem. Phys., **73**, 1143 (1980).
[61] P. Michaud and R.J. Cvetanovic, J. Phys. Chem., **76**, 1375 (1972) and references therein.
[62] R.K. Sparks, L.R. Carlson, K. Shobatake, M.L. Kowalczyk and Y.T. Lee, J. Chem. Phys., **72**, 1491 (1980).
[63] J. Glownia, J. Misewich, R. Walkup, M. Kaschke and P. Sorokin, Top. Appl. Phys. **70**, 3 (1992).
[64] A.H. Zewail, J. Phys. Chem., **100**, 12701 (1996).
[65] A.H. Zewail, Science, **242**, 1645 (1988).
[66] C. Leforestier, F. LeQuere, K. Yamashita and K. Morokuma, J. Chem. Phys., **101**, 3806 (1994).
[67] N. Balakrishnan and G.D. Billing, J. Chem. Phys., **101**, 2968 (1994).
[68] D. Chasman, D.J. Tannor and D.G. Imre, J. Chem. Phys., **89**, 6667 (1988).
[69] A.G. Suits, R.L. Miller, L.S. Bontuyan and P.L. Houston, J. Chem. Soc. Faraday Trans., **89**, 1443 (1993).
[70] J.J. Knudtson and J.C. Stephenson, Chem. Phys. Lett., **107**, 385 (1984) and works cited therein.
[71] C. Lugez, A. Schriver, R. Levant and L. Schriver-Mazzuoli, Chem. Phys. **181**, 129 (1994).
[72] P.M. Aker, J.J.A. O'Brien and J.J. Sloan, J. Chem. Phys., **84**, 745 (1986).
[73] S.G. Cheskis, A.A. Iogansen, P.V. Kulakov, I. Yu. Razuvaev, O.M. Sarkisov and A.A. Titov, Chem. Phys. Letters, **155**, 37 (1989).
[74] Y. Hurwitz, Y. Rudich and R. Naaman, Chem. Phys. Letters, **215**, 674 (1993).
[75] Y. Rudich, Y. Hurwitz, G.J. Frost, V. Vaida and R. Naaman, J. Chem. Phys., **99**, 4500 (1993).
[76] P. Andresen and A.C. Luntz, J. Chem. Phys., **72**, 5842 (1980).
[77] G.M. Sweeney, A. Watson and K.G. McKendrick, J. Chem. Phys., **106**, 9172 (1997).
[78] J. McFarlane, J.C. Polanyi and J.G. Shapter, J. Photochem. Photobiol., **A58**, 139 (1991).
[79] S.P. Walsh and T.H. Dunning, Jr., J. Chem. Phys., **72**, 3221 (1980).

[80] D.C. Clary, Phys. Chem. Chem. Phys., **1**, 1173 (1999).
[81] J.C. Corchado, J.E.-Garcia, O.R.-Neto, Y.-Y. Chuang and D.G. Truhlar, J. Phys. Chem., **102**, 4899 (1998).
[82] M. González, J. Hernando, J. Millán and R. Sayós, J. Chem. Phys., **110**, 7326 (1999).
[83] G.M. Sweeney and K.G. McKendrick, J. Chem. Phys., **106**, 9182 (1997).
[84] P. Casavecchia, R.J. Buss, S.J. Sibener and Y.T. Lee, J. Chem. Phys., **73**, 6351 (1980).
[85] I.-C. Chen, W.H. Green, Jr. and C. Bradley Moore, J. Chem. Phys., **89**, 314, (1988).
[86] P.R. Bunker, P. Jensen, W.P. Kraemer and R. Beardsworth, J. Chem. Phys., **85**, 3724 (1986).
[87] S. Dóbé, T. Bérces, F. Temps, H. Gg. Wagner and H. Ziemer, J. Phys. Chem., **98**, 9792 (1994).
[88] C.-F. Pau and W.J. Hehre, J. Phys. Chem., **86**, 1252, (1982).
[89] R.D. Johnson III and J.W. Hudgens, J. Phys. Chem., **100**, 19874 (1996).
[90] J.C. Stephenson, J.A. Blazy, C.-L. Li and D.S. King, J. Chem. Phys., **76**, 5989 (1982).
[91] J.C. Stephenson and D.S. King, J. Chem. Phys., **78**, 1867 (1982).
[92] S.E. Bialkowski and W.A. Guillory, J. Chem. Phys., **68**, 3339 (1977).
[93] R. Schmiedl, U. Meier and K.H. Welge, Chem. Phys. Letters, **80**, 495 (1981).
[94] The program "A General RRKM Program", by W.L. Hase and D.L. Bunker, QCPE No. 234, was used to calculate RRKM rates for dissociation of CH_3OH. Transition state frequencies of 3682, 2947(2), 2846, 1479, 1455, 1427, 400, 300, 280 cm^{-1}, and TRM=TRC=7.5x10-3 amu nm^2 were chosen, which fit the 5.4 ps lifetime for the cluster experiment, the IRMPD timescales, and the Arrhenius A factor of $.10^{16}s^{-1}$.
[95] W. Tsang, Int'l. J. of Chem. Kinetics, **8**, 193 (1976).
[96] D.S. King, in *Dynamics of the Excited State*, edited by K.P.Lawley (Wiley, New York, 1982).
[97] J.C. Stephenson, M.P. Casassa and D.S. King, J. Chem. Phys. **89**, 1378 (1988).